

# A Synthetic Photorespiratory Shortcut Enhances Photosynthesis to Boost Biomass and Grain Yield in Rice

Li-Min Wang<sup>1,2,3</sup>, Bo-Ran Shen<sup>1,3</sup>, Bo-Di Li<sup>1</sup>, Chuan-Ling Zhang<sup>1</sup>, Min Lin<sup>1</sup>, Pan-Pan Tong<sup>1</sup>, Li-Li Cui<sup>1</sup>, Zhi-Sheng Zhang<sup>1</sup> and Xin-Xiang Peng<sup>1,\*</sup>

<sup>1</sup>State Key Laboratory for Conservation and Utilization of Subtropical Agro-Bioresources, College of Life Sciences, South China Agricultural University, Guangzhou 510642, China

<sup>2</sup>College of Agriculture and Biology, Zhongkai University of Agriculture and Engineering, Guangzhou, China

<sup>3</sup>These authors contributed equally to this article.

\*Correspondence: Xin-Xiang Peng ([xpeng@scau.edu.cn](mailto:xpeng@scau.edu.cn))

<https://doi.org/10.1016/j.molp.2020.10.007>

## ABSTRACT

Several photorespiratory bypasses have been introduced into plants and shown to improve photosynthesis by increasing chloroplastic CO<sub>2</sub> concentrations or optimizing energy balance. We recently reported that an engineered GOC bypass could increase photosynthesis and productivity in rice. However, the grain yield of GOC plants was unstable, fluctuating in different cultivation seasons because of varying seed setting rates. In this study, we designed a synthetic photorespiratory shortcut (the GCGT bypass) consisting of genes encoding *Oryza sativa* glycolate oxidase and *Escherichia coli* catalase, glyoxylate carboligase, and tartronic semialdehyde reductase. The GCGT bypass was guided by an optimized chloroplast transit peptide that targeted rice chloroplasts and redirected 75% of carbon from glycolate metabolism to the Calvin cycle, identical to the native photorespiration pathway. GCGT transgenic plants exhibited significantly increased biomass production and grain yield, which were mainly attributed to enhanced photosynthesis due to increased chloroplastic CO<sub>2</sub> concentrations. Despite the increases in biomass production and grain yield, GCGT transgenic plants showed a reduced seed setting rate, a phenotype previously reported for the GOC plants. Integrative transcriptomic, physiological, and biochemical assays revealed that photosynthetic carbohydrates were not transported to grains in an efficient manner, thereby reducing the seed setting rate. Taken together, our results demonstrate that the GCGT photorespiratory shortcut confers higher yield by promoting photosynthesis in rice, mainly through increasing chloroplastic CO<sub>2</sub> concentrations.

**Key words:** photorespiratory shortcut, photosynthesis, yield, rice

**Wang L.-M., Shen B.-R., Li B.-D., Zhang C.-L., Lin M., Tong P.-P., Cui L.-L., Zhang Z.-S., and Peng X.-X. (2020). A Synthetic Photorespiratory Shortcut Enhances Photosynthesis to Boost Biomass and Grain Yield in Rice. Mol. Plant. **13**, 1802–1815.**

## INTRODUCTION

Increasing crop yield is the ultimate way to meet the challenge of doubling global food production by 2050 (Tilman et al., 2011; Ray et al., 2013; Long et al., 2015; South et al., 2018). Yield is highly correlated with biomass, which is mainly determined by photosynthetic efficiency (Heyneke and Fernie, 2018). Therefore, scientists predict that in the first half of the twenty-first century, there will be a second green revolution centered on further improvements to photosynthetic efficiency (Long et al., 2006, 2015; Zhu et al., 2008; Von Caemmerer et al., 2012). Photorespiration, in which O<sub>2</sub> is taken up in a light-dependent manner and CO<sub>2</sub> is simultaneously released, has

long been known to be a powerful regulator of photosynthesis (Bauwe et al., 2010; Betti et al., 2016). Photorespiration is the end result of an oxygenation reaction catalyzed by ribulose-1,5-bisphosphate carboxylase/oxygenase. During this metabolic process, CO<sub>2</sub> and NH<sub>3</sub> are released in mitochondria, and ATP and reducing equivalents are consumed (Wingler et al., 2000; Peterhansel et al., 2013a). In C<sub>3</sub> plants, little of the CO<sub>2</sub> that is released in mitochondria can re-enter the Calvin cycle for reuse, causing a 25%–30% reduction in the carbon fixed by

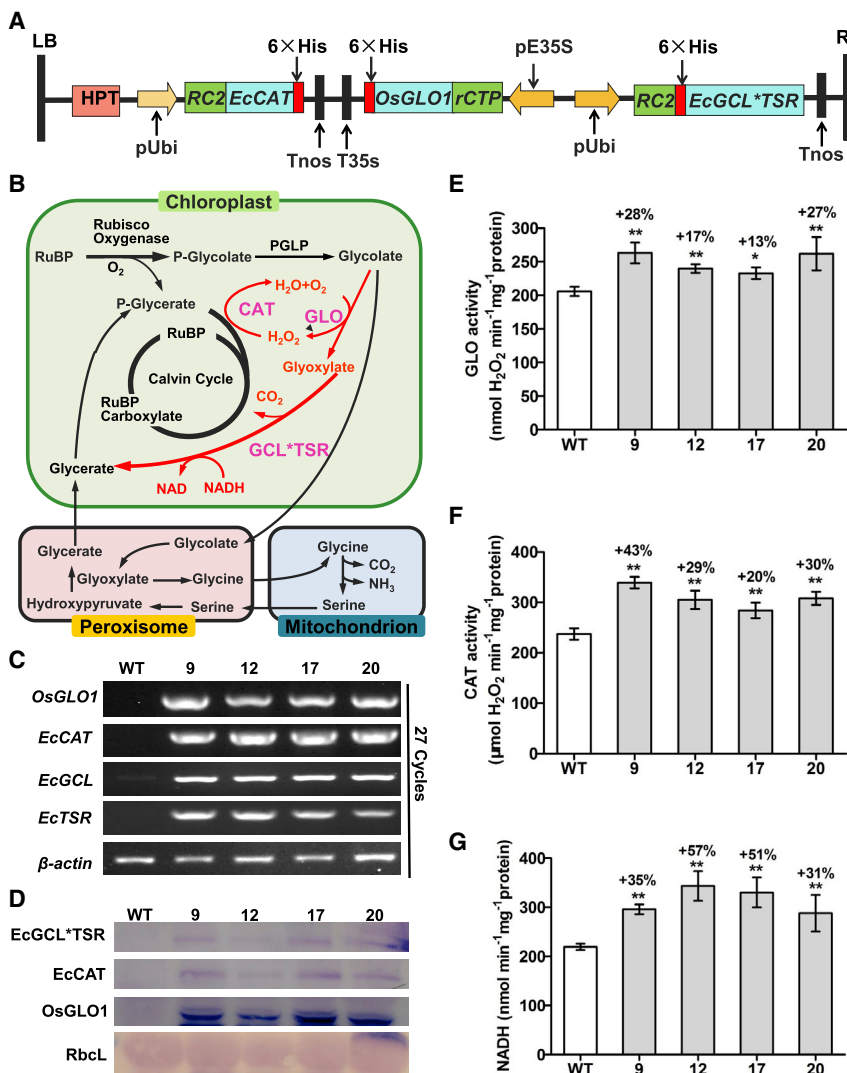


**Figure 1. Identification and Verification of Transgenic Rice Plants Carrying the GCGT Bypass.**

**(A)** Structure of the multi-gene expression vector GCGT-pYL1305. pE35S, CaMV 35S enhanced promoter; T35S, CaMV 35S terminator; pUbi, *ubi* promoter; Tnos, *nos* terminator; HPT, expression cassette of *hygromycin phosphotransferase* gene; LB, left border; and RB, right border.

**(B)** The newly designed GCGT bypass (in red) is illustrated, along with the plant photorespiration pathway (in black). The introduced enzymes are indicated in purple. RuBP, ribulose-1,5-bisphosphate; PGLP, phosphoglycolate phosphatase; GLO, *OsGLO1*, rice glycolate oxidase isoform one; CAT, *Escherichia coli* catalase; GCL, *E. coli* glyoxylate carboligase; TSR, *E. coli* tartronic semialdehyde reductase.

**(C)** Total RNA extracted from the leaves of wild-type (WT) and four transgenic lines was used for RT-PCR analysis with gene-specific primers as listed in [Supplemental Table 1](#); the rice *β-actin* gene served as the endogenous control.

**(D)** Total protein extracted from the leaves of WT and transgenic lines was analyzed by Western blot analysis. OsGLO1, EcCAT, and EcGCL\*TSR were detected by a His monoclonal antibody, and the staining of the large subunit of Rubisco with Ponceau S served as the control.

**(E–G)** Analyses of GLO and CAT activities; **(G)** analysis of GCL and TSR activities by a coupled assay.

Data are presented as the mean  $\pm$  SD;  $n = 4$ ; \* $P < 0.05$ ; \*\* $P < 0.01$ , according to one-way ANOVA followed by a Tukey's *post hoc* test for mean comparisons. ANOVA tables for each analysis are shown in [Supplemental Data 5](#).

photosynthesis (Somerville, 2001). Under hot and dry growth conditions, photorespiration may further increase, resulting in even more carbon loss (Peterhansel et al., 2010; Long et al., 2015). If photorespiration were eradicated, it is predicted that photosynthesis would increase by 12%–55% (Peterhansel and Maurino, 2011; Walker et al., 2016a). Thus, there is great potential for improving photosynthetic efficiency by reducing photorespiration.

Several photorespiratory bypasses have been designed and tested in plants over the past few years. Kebeish et al. (2007) designed the first bypass (bypass 1) by introducing *Escherichia coli* glycolate dehydrogenase (GlycolateDH), glyoxylate carboligase (EcGCL), and tartronic semialdehyde reductase (EcTSR) into *Arabidopsis* chloroplasts; 75% of glycolate fed into this bypass was returned to the Calvin cycle (Kebeish et al., 2007). In bypass 2, two *E. coli* enzymes, EcGCL and hydroxypyruvate isomerase (HYI), were introduced into peroxisomes to catalyze the conversion of glyoxylate into hydroxypyruvate with the release of CO<sub>2</sub> in peroxisomes (Carvalho et al., 2011). In bypass 3, glycolate was completely oxidized to CO<sub>2</sub> in chloroplasts by both

newly introduced (glycolate oxidase, malate synthase, and catalase) and endogenous (NADP-malic enzyme and pyruvate dehydrogenase) enzymes (Maier et al., 2012). Transgenic plants with bypass 1 or bypass 3 have increased photosynthesis and biomass yield under low-light and short-day conditions (Kebeish et al., 2007; Maier et al., 2012), but no positive effects were detected for plants with bypass 2 (Carvalho et al., 2011). Subsequently, the introduction of bypass 1 or a portion of bypass 1 into potato (*Solanum tuberosum*), *Camellia sativa*, and tobacco (*Nicotiana tabacum*) was found to increase photosynthesis, biomass yield, and tuber/seed yield (Nölke et al., 2014; Dalal et al., 2015; South et al., 2019). In bypass 4, glycolate dehydrogenase from *Chlamydomonas reinhardtii* and malate synthase from *Cucurbita maxima* are redirected to the chloroplasts of tobacco plants, while the plastidial glycolate exporter PLGG1 is silenced to restrict the export of glycolate from chloroplasts (South et al., 2019). Although no positive effects on photosynthesis or biomass yield were observed when bypass 3 was introduced into tobacco, the introduction of bypass 4 resulted in a biomass increase of 40% compared with wild-type (WT) plants under field conditions (South et al., 2019). We recently engineered a new

photorespiratory bypass known as the GOC bypass (or bypass 5) in rice (*Oryza sativa*) chloroplasts. This bypass is characterized by the production of no reducing equivalents during the complete oxidation of glycolate into CO<sub>2</sub>, which is catalyzed by three rice enzymes, glycolate oxidase (OsGLO3), oxalate oxidase (OsOXO3), and catalase (OsCATC). Rice plants carrying the GOC bypass showed significant increases in photosynthesis efficiency and grain yield (Shen et al., 2019). In terms of energy metabolism, the GOC bypass resembles bypass 3: glycolate is completely oxidized to CO<sub>2</sub> without reconnection to the native photorespiratory pathway (Maier et al., 2012; Shen et al., 2019). However, the GOC bypass shows an obvious advantage in that there are more benefits from the increased chloroplast CO<sub>2</sub> concentration (Cc) than from the improved energy balance (Peterhansel et al., 2013a; Shen et al., 2019).

We had previously tried a synthetic photorespiratory shortcut, which was essentially similar to bypass 1 reported by Kebeish et al. (2007) and consisted of genes encoding *Cyanobacteria* glycolate dehydrogenase (SyGDH), *Escherichia coli* glyoxylate carboligase (EcGCL), and tartronic semialdehyde reductase (EcTSR). However, the introduction of this shortcut into rice plants resulted in little accumulation of the exogenous proteins in chloroplasts. A subsequent investigation revealed that rice rbcS (ribulose-1,5-bisphosphate carboxylase/oxygenase small subunit) chloroplast transit peptide (rCTP) could not target EcGCL and EcTSR to rice chloroplasts, resulting in the degradation of these proteins within cells (Shen et al., 2017). We therefore generated an optimized rCTP, RC2, which has been shown to more effectively target diverse proteins into rice chloroplasts (Shen et al., 2017). In this study, we used RC2 to once again introduce a synthetic photorespiratory shortcut into rice chloroplasts, which consisted of genes encoding rice glycolate oxidase (OsGLO1) and *E. coli* catalase (EcCAT), EcGCL, and EcTSR. This shortcut was designated as the GCGT bypass. Because it could recover 3/4 of the photorespiratory glycolate into the Calvin cycle—unlike the GOC bypass, which oxidizes all the glycolate into CO<sub>2</sub>—we expected that this shortcut would be more efficient in increasing photosynthesis and productivity. We also hoped that the issue of reduced seed setting rate encountered with the GOC bypass would be improved with the GCGT shortcut.

## RESULTS

### A Synthetic Photorespiratory Shortcut Was Designed and Successfully Established in Rice

We designed a synthetic photorespiratory shortcut that consisted of genes encoding OsGLO1, EcCAT, EcGCL, and EcTSR and designated it the GCGT bypass. We used RC2 to guide the GCGT bypass into chloroplasts and introduced the bypass into rice plants via *Agrobacterium*-mediated transformation. In the GCGT bypass, a portion of the glycolate produced by photorespiration was directly metabolized to produce CO<sub>2</sub> inside chloroplasts; the H<sub>2</sub>O<sub>2</sub> produced by glycolate oxidation was decomposed by EcCAT, and two glycolates were converted to one glycerate by EcGCL and EcTSR, with the release of one CO<sub>2</sub> (Figure 1B). Glycolate oxidase (GLO) is a key enzyme in photorespiratory metabolism. Five GLO isozymes (OsGLO1 to

### Photorespiratory Shortcut Enhances Photosynthesis

OsGLO5) have been identified in rice, with OsGLO1 having the most important role (Zhang et al., 2012); it was therefore recruited for use in the GCGT bypass. OsCAT was used in the GOC bypass, and its activity was regulated by a chaperone protein (NCA1a and NCA1b) that maintained the folding of CAT. Both NCA1a and NCA1b were localized in the cytosol (Liu et al., 2019), which may affect OsCAT activity in chloroplasts. Therefore, EcCAT was used in the GCGT bypass to decompose H<sub>2</sub>O<sub>2</sub> without the requirement of a chaperone protein. To coordinate the expression of GCL and TSR, and to use fewer promoters, we created a fusion protein by linking EcGCL and EcTSR with a 3(Gly3Ser2) linker (referred to as EcGCL\*TSR hereafter) (Supplemental Figure 1). EcGCL\*TSR showed catalytic activity similar to those of GCL and TSR alone (Supplemental Figure 2). Similar to native photorespiration, the GCGT bypass could recover 75% of carbon from glycolate metabolism into the Calvin cycle (Kebeish et al., 2007; Peterhansel et al., 2013a), whereas our previously created GOC bypass completely oxidized glycolate to CO<sub>2</sub> without reconnection to the major photorespiratory pathway. The GCGT bypass is therefore considered a photorespiratory shortcut. In addition, there were three reactions producing H<sub>2</sub>O<sub>2</sub> in the GOC bypass but only one in the GCGT bypass. The energy balance of the GCGT bypass was similar to that of native photorespiration, whereas bypass 1 showed an improved energy balance (Peterhansel et al., 2013a). By using a fusion protein (EcGCL\*TSR) and a multi-gene expression vector in the GCGT bypass, four target genes were introduced into rice simultaneously, making it easy to obtain homozygous lines. By contrast, bypass 1 transgenic plants with five target genes (including the three subunits of glycolate dehydrogenase) were obtained by crossing GT and DEF plants, and it was therefore difficult to obtain homozygous lines (Kebeish et al., 2007).

GCGT-pYL1305, which contained OsGLO1, EcCAT, EcGCL, and EcTSR, was constructed (Figure 1A); the expression of EcCAT and EcGCL\*TSR was driven by pUBI (corn ubiquitin gene promoter), and the expression of OsGLO1 was driven by pE35S (enhanced CaMV 35S promoter). OsGLO1 was fused with rCTP, and EcCAT and EcGCL\*TSR were fused with RC2, which had been shown to more effectively target EcCAT, EcGCL, and EcTSR into rice chloroplasts (Shen et al., 2017). GCGT-pYL1305 was then transformed into rice via *Agrobacterium*-mediated transfection, and several independent homozygous lines were identified. Four independent homozygous lines, namely GCGT 9, 12, 17, and 20, were used for detailed analyses in this study. Expression analyses showed that the four target genes were well expressed at the RNA (Figure 1C) and protein (Figure 1D) levels, and all enzymes exhibited high activity (Figure 1E–1G). GLO activity was 13%–28% higher in GCGT transgenic plants than in WT plants (Figure 1E), and CAT activity was 20%–43% higher in GCGT transgenic plants than in WT plants (Figure 1F). The activities of GCL and TSR were tested using a coupled assay; GCL produces tartronic semialdehyde as a substrate for the TSR reaction, which in turn uses NADH as a cofactor. NADH consumption, which depends on the activities of GCL and TSR, was 31%–57% higher in GCGT transgenic plants than in WT plants (Figure 1G). These results demonstrated that the GCGT bypass was successfully installed in rice chloroplasts.

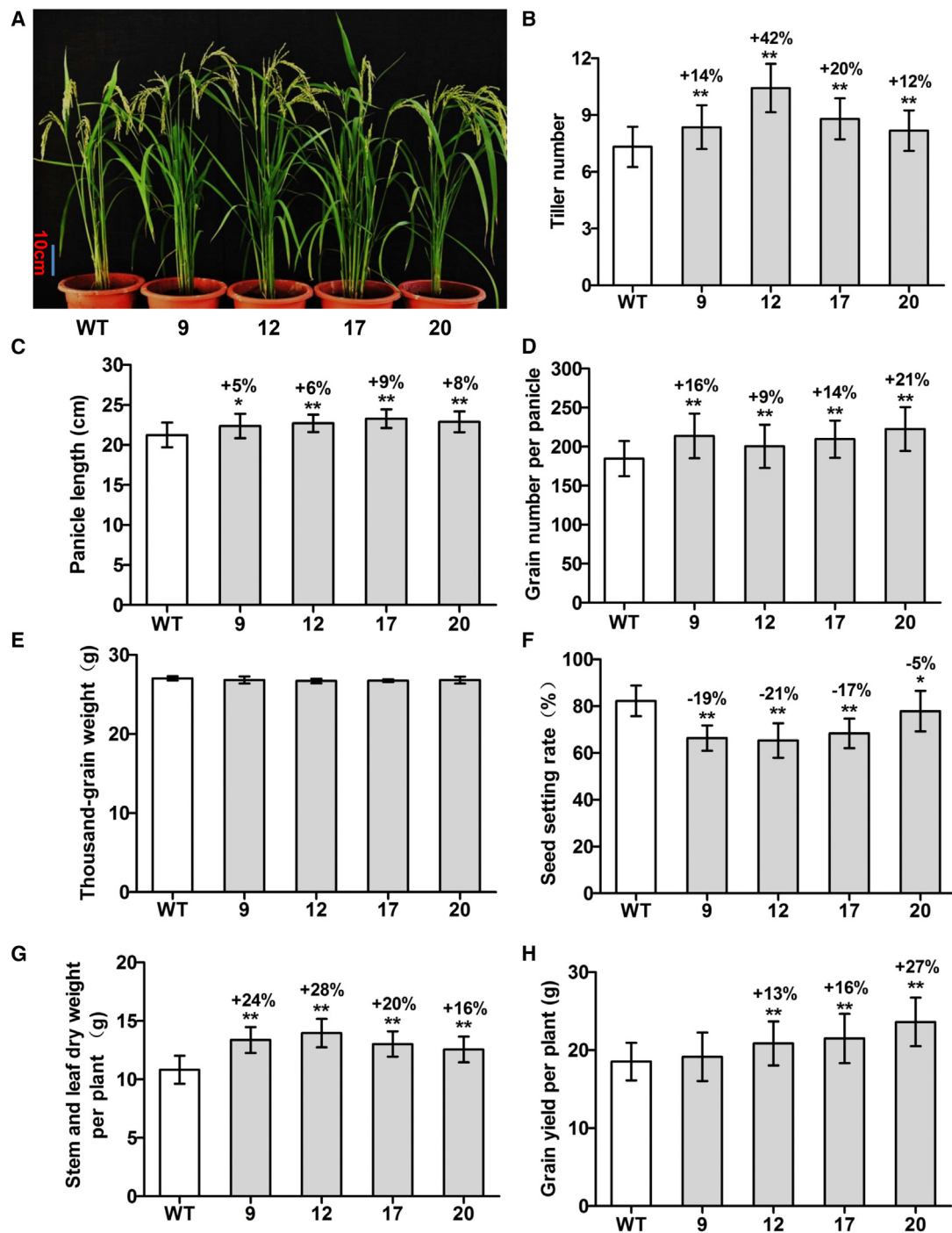


**Figure 2. Growth Traits, Biomass Production, and Grain Yield of GCGT Transgenic Plants.**

(A) A representative photograph of GCGT transgenic plants grown in the field. Plants were transferred to pots at the filling stage and photographed. (B–H) Quantification of tiller number (B), panicle length (C), grain number per panicle (D), thousand-grain weight (E), seed setting rate (F), stem and leaf dry weight per plant (G), and grain yield per plant (H).

Data are presented as the mean  $\pm$  SD;  $n = 100$ ; \* $P < 0.05$ ; \*\* $P < 0.01$ , according to one-way ANOVA followed by a Tukey's post hoc test for mean comparisons. ANOVA tables for each analysis are shown in [Supplemental Data 5](#).

#### Biomass and Grain Yield Are Significantly Increased in GCGT Transgenic Plants

GCGT transgenic plants were grown in the field to determine growth traits, biomass, and grain yield. GCGT transgenic plants

appeared larger than WT plants (Figure 2A). Tiller numbers of the GCGT lines were 12%–42% higher than those of WT plants (Figure 2B). Furthermore, the main panicles were 5%–9% longer, and the grain numbers per main panicle were 9%–21% higher in GCGT plants than in WT plants; however, there was

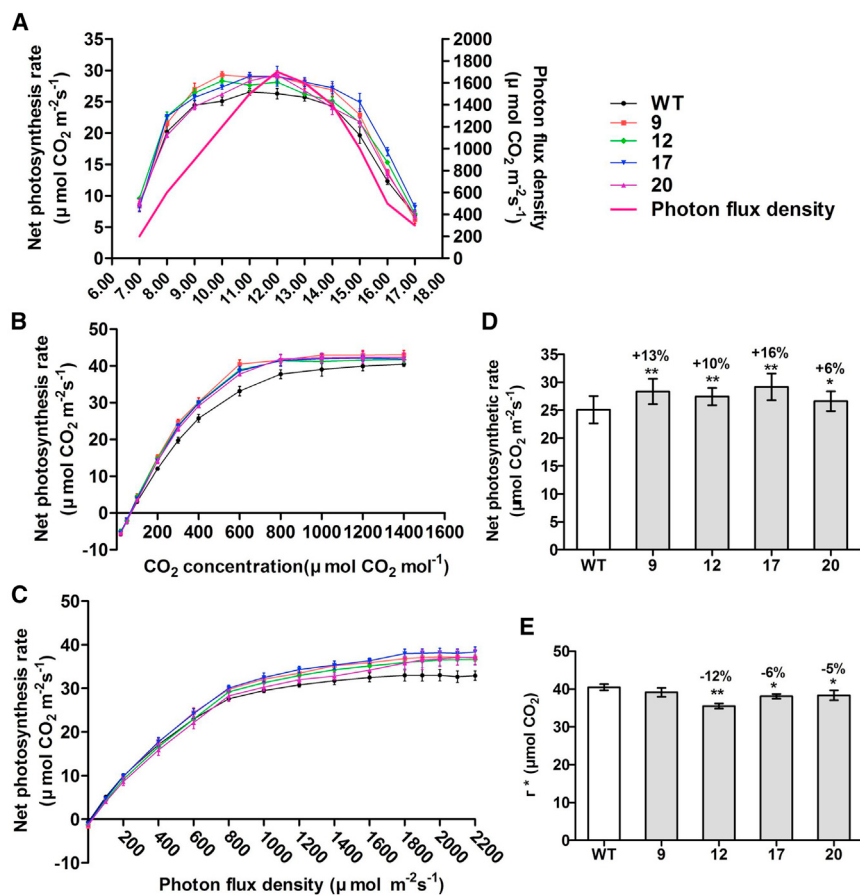


**Figure 3. Photosynthetic Parameters for GCGT and WT Plants.**

All measurements were performed using flag leaves of rice at the filling stage.

(A) Diurnal curves of the net photosynthetic rate were generated in October at a temperature of 30°C, a CO<sub>2</sub> concentration of approximately 400 ppm, and relative humidity of 50%–75%; n = 5.

(B) CO<sub>2</sub> response curves were generated at a photon flux density (PFD) of 1000 μmol m<sup>-2</sup> s<sup>-1</sup> and a temperature of 30°C; n = 5.

(C) Light response curves were generated at a temperature of 30°C under normal air conditions and a CO<sub>2</sub> concentration of approximately 400 ppm; n = 5.

(D) The net photosynthetic rate was measured at a PFD of 1000 μmol m<sup>-2</sup> s<sup>-1</sup>, a temperature of 30°C, and a CO<sub>2</sub> concentration of approximately 400 ppm; n = 30.

(E)  $\Gamma^*$  (CO<sub>2</sub> compensation point) was measured using the Laisk method, and the curves were analyzed using the linearization method of Walker et al. (2016b); n = 4.

Data are presented as the mean  $\pm$  SD; \*P < 0.05; \*\*P < 0.01, according to one-way ANOVA followed by a Tukey's post hoc test for mean comparisons. ANOVA tables for each analysis are shown in [Supplemental Data 5](#).

no significant difference in thousand-grain weight (Figure 2C–E). The aboveground dry weights of GCGT plants harvested at the maturation stage were 16%–28% higher than those of WT plants (Figure 2G). The seed setting rates of GCGT lines were 5%–21% lower than those of WT plants (Figure 2F), similar to previously reported observations in GOC rice plants (Shen et al., 2019). Despite the decreased seed setting rate, the grain yield per plant was still significantly higher in GCGT transgenic plants than in WT plants, with increases ranging from 13% to 27%. This was mainly due to increases in tiller number, panicle length, and grain number per main panicle (Figure 2H).

### Photosynthetic Efficiency and Capacity Are Largely Improved in GCGT Transgenic Plants

#### Photosynthetic Rates

We measured gas exchange in GCGT and WT plants. Diurnal curves of the net photosynthetic rate (Pn) showed that the Pn of GCGT plants was significantly higher than that of WT plants during most of the day (Figure 3A), with the average increase ranging from 6% to 16% for four independent lines (Figure 3D). To further confirm the increased photosynthesis, light response and CO<sub>2</sub> response curves were generated. No significant difference in Pn was observed between GCGT and WT plants when the photon flux density (PFD) was lower than 400 μmol m<sup>-2</sup> s<sup>-1</sup>; however, a difference emerged when the PFD was higher than 400 μmol m<sup>-2</sup> s<sup>-1</sup>, with Pn peaking

at approximately 1600 μmol m<sup>-2</sup> s<sup>-1</sup> (Figure 3C). GCGT transgenic plants also had higher Pn values compared with those of WT plants at different intracellular CO<sub>2</sub> concentrations (Figure 3B). Carboxylation efficiency was significantly increased in GCGT plants, and the apparent CO<sub>2</sub> compensation point calculated from A/Ci curves was significantly lower in transgenic plants compared with WT (Supplemental Table 2). The light saturation point (LSP) and A<sub>max</sub> (light-saturated Pn) were both significantly higher in GCGT plants, whereas the apparent quantum yield (AQE) and the maximum quantum efficiency of photosystem II ( $F_v/F_m$ ) were similar between GCGT and WT plants (Supplemental Table 2). The  $\Gamma^*$  (CO<sub>2</sub> compensation point calculated using the common intercept method and slope regression according to Walker et al. [2016b]) of GCGT plants was significantly decreased by 5%–12% (Figure 3E), suggesting improved CO<sub>2</sub> refixation (Peterhansel et al., 2013a).

#### Increased Photosynthetic Carbohydrate Content and Chloroplast Size in Leaves

We further analyzed the photosynthetic carbohydrate content in the leaves of GCGT and WT plants. Starch contents in leaves of GCGT 9, 12, 17, and 20 lines were 21%–62% and 35%–102% higher than those in WT plants at the heading and filling stages, respectively (Figure 4A). Sucrose contents were 16%–29% higher in GCGT plants than in WT plants at the heading stage and 33%–53% higher at the filling stage (Figure 4B). The glucose and fructose contents in leaves of GCGT 9, 12, and 17 lines were 24%–74% and 24%–80% higher, respectively, than those in WT leaves at the filling stage (Supplemental Figure 3).

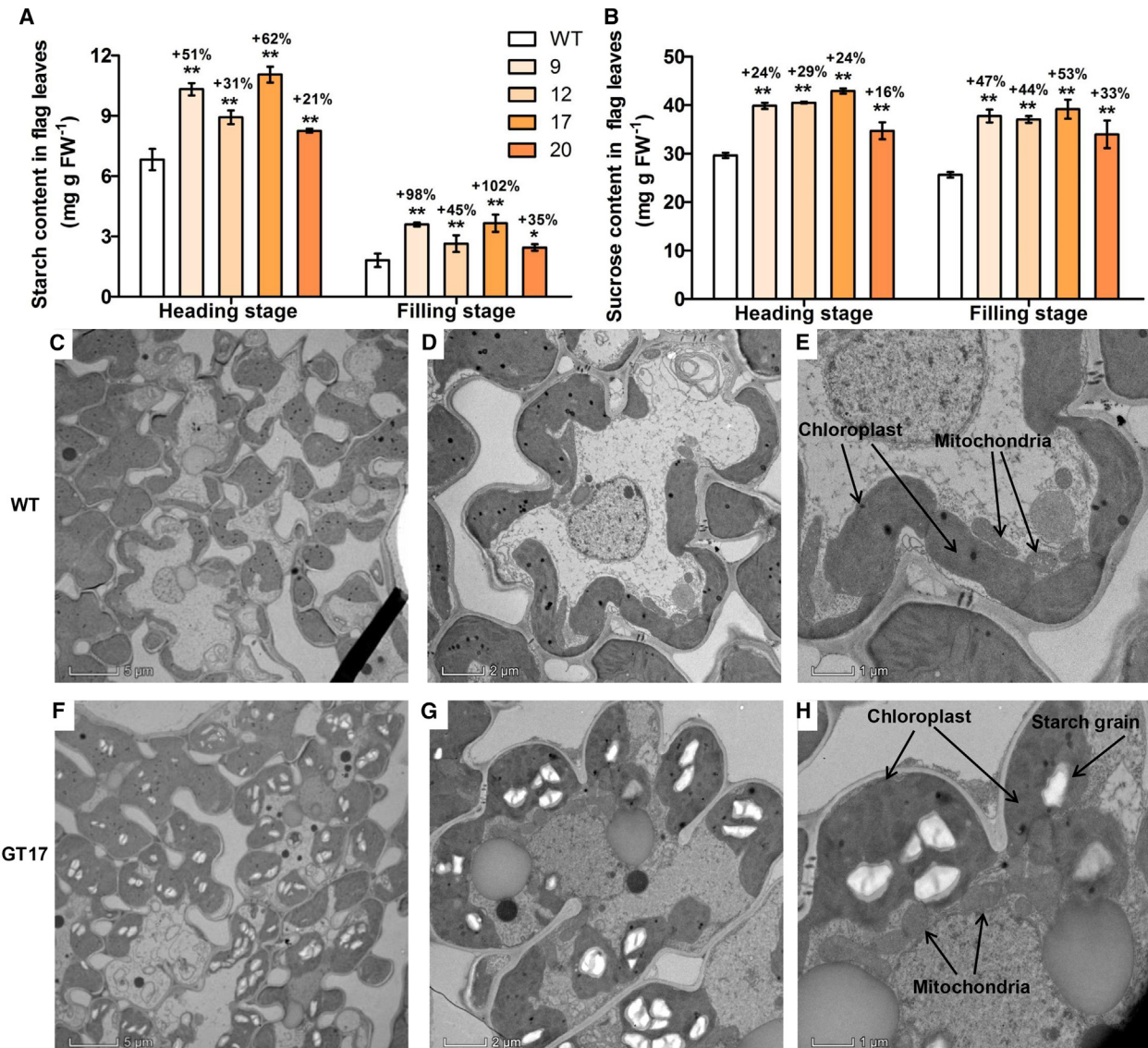


**Figure 4. Photosynthetic Carbohydrate Content and Electron Micrographs of Leaves of GCGT and WT Plants.**

(A) The starch content in flag leaves.

(B) The sucrose content in flag leaves. Data are presented as the mean  $\pm$  SD;  $n = 4$ ; \* $P < 0.05$ ; \*\* $P < 0.01$ , according to one-way ANOVA followed by a Tukey's post hoc test for mean comparisons. ANOVA tables for each analysis are shown in [Supplemental Data 5](#).

(C-E) Transmission electron micrographs of leaves in WT plants at the filling stage.

(F-H) Transmission electron micrographs of leaves in GCGT 17 at the filling stage. Each image is representative of four independent plants.

The ultrastructure of flag leaves and sheaths was observed by transmission electron microscopy at the filling stage. In flag leaves, the sizes of mesophyll cells and chloroplasts were increased by 21.17% and 110.9%, respectively, in GCGT line 17 compared with WT (Figure 4C–4H and [Supplemental Table 3](#)). Chloroplasts occupied most of the cell space, but the numbers of chloroplasts were not significantly different between GCGT 17 and WT plants ([Supplemental Table 3](#)). Chloroplasts in leaf sheaths also appeared significantly larger, occupying most of the cell space ([Supplemental Figure 4](#)). Consistent with the increased starch content (Figure 4A), the number of starch grains was significantly higher in GCGT 17 than in WT plants (Figure 4C–4H and [Supplemental Table 3](#)). The number of mitochondria

did not differ significantly between GCGT 17 and WT plants ([Supplemental Table 3](#)).

#### Suppression of Photorespiration via Photosynthetic CO<sub>2</sub> Concentration Leads to Increased Photosynthesis

The CO<sub>2</sub> concentration inside chloroplasts (Cc) is a critical parameter, as it indicates whether the CO<sub>2</sub> concentrating mechanism has indeed been established in transgenic plants. Here, the Cc was determined using the variable J method described by Harley et al. (1992). Cc was 9%–12% higher in GCGT transgenic plants than in WT plants (Figure 5A), whereas the photorespiration rate was reduced by 14%–19% (Figure 5B). We also used gas chromatography followed by

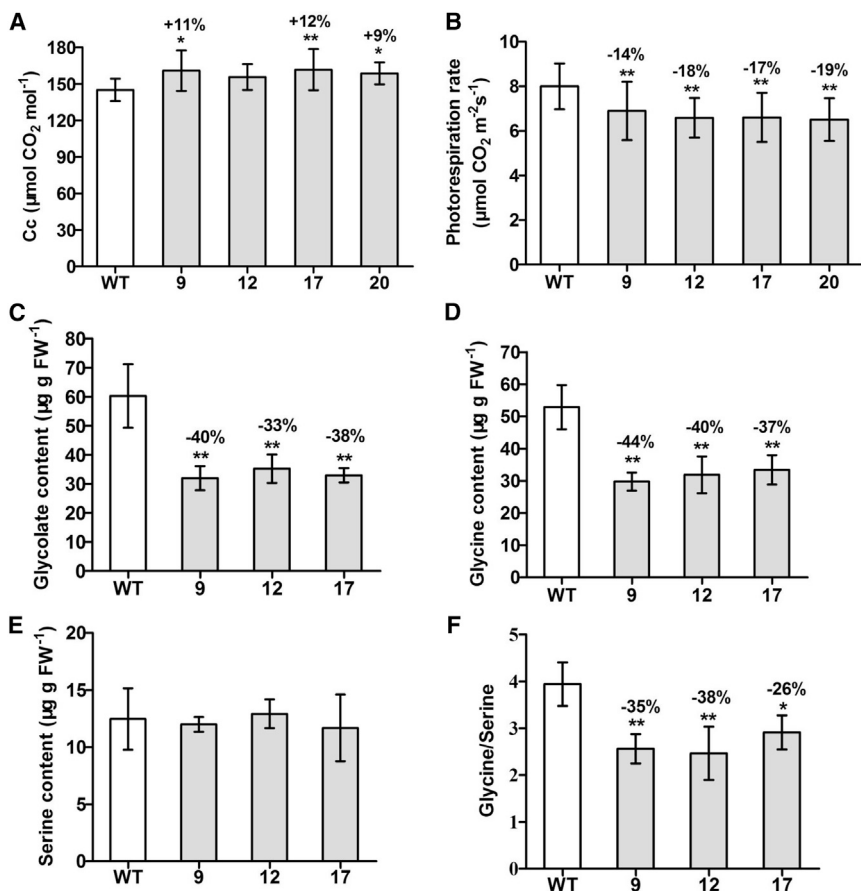


**Figure 5. Chloroplast  $\text{CO}_2$  Concentrations and Photorespiratory Metabolite Contents in GCGT Transgenic Plants.**

All measurements were performed using flag leaves of rice at the filling stage.

(A) The chloroplast  $\text{CO}_2$  concentration ( $\text{Cc}$ ) was measured using the variable  $J$  method as described by Harley et al. (1992);  $n = 5$ .

(B) The photorespiration rate was measured using the low  $\text{O}_2$  method with a PFD of  $1000 \mu\text{mol m}^{-2} \text{ s}^{-1}$ , a temperature of  $30^\circ\text{C}$ , and a  $\text{CO}_2$  concentration of approximately 400 ppm;  $n = 30$ .

(C) Glycolate content.

(D) Glycine content.

(E) Serine content.

(F) Glycine/serine ratio.

In (C)–(F)  $n = 4$ . Data are presented as the mean  $\pm$  SD; \* $P < 0.05$ ; \*\* $P < 0.01$ , according to one-way ANOVA followed by a Tukey's post hoc test for mean comparisons. ANOVA tables for each analysis are shown in [Supplemental Data 5](#).

mass spectrometry (GC-MS) to analyze the contents of photorespiratory intermediates, namely glycolate, glycine, and serine, under photorespiratory conditions (sampled at 14:00). A significant decrease in glycolate level was observed in GCGT plants compared with WT plants (Figure 5C). In addition, GCGT transgenic plants had lower glycine levels and lower glycine/serine ratios (Figure 5D–5F). Glycine and serine levels indicate the carbon flux during photorespiration (Berry et al., 1978), and lower ratios of glycine/serine may reveal reduced photorespiration (Novitskaya et al., 2002; Kebeish et al., 2007; Shen et al., 2019). Taken collectively, these data strongly suggest that the flow of carbon through the native photorespiratory pathway in GCGT transgenic plants has been successfully split, with a portion released as  $\text{CO}_2$  inside the chloroplasts, leading to increased  $\text{Cc}$ .

### Carbohydrate Accumulation and Transport in Relation to Reduced Seed Setting Rate

#### Accumulation of Carbohydrates in Stems

During the vegetative and early reproductive stages of rice, carbon assimilates are temporarily stored in stems and leaf sheaths as non-structural carbohydrates and subsequently transported to developing grains at the filling stage (Scofield et al., 2009). We measured sucrose and starch contents in stems (culms and sheaths) at the heading and filling stages because they are known to function in the transport and storage of carbohydrates in plants, respectively. The sucrose content in the

stems of GCGT lines was 10%–32% higher than in those of WT plants at the heading stage and 16%–207% higher at the filling stage (Figure 6A). Similarly, the starch content was 26%–68% higher in the stems of GCGT lines at the heading stage and 67%–418% higher at the filling stage compared with corresponding controls (Figure 6B). Therefore, GCGT transgenic plants accumulated more photosynthates in the stem at the filling stage. To more clearly show the change in sucrose and starch transport in stems from the heading to the filling stage, we calculated the apparent ratios of transferred stem sucrose and starch. For sucrose, the ratios were 13%, 41%, and 46% lower in GCGT lines 9, 12, and 17 than in WT plants (Figure 6C); for starch, they were 87%, 88%, 89%, and 14% lower in GCGT lines 9, 12, 17, and 20 than in WT plants (Figure 6D). These data suggest that photosynthetic carbohydrates in the stems of GCGT plants were not transported to grains at the filling stage in a timely and efficient manner.

#### Transcriptomic Changes in Relation to Carbohydrate Metabolism and Transport

RNA sequencing (RNA-seq) analysis was conducted to evaluate the changes in gene expression induced by the introduction of the GCGT bypass. Stems (culms and sheaths) sampled from GCGT 12, 17, and 20 lines and WT plants at the filling stage were used for RNA-seq analysis. A total of 2028 genes in stems were differentially expressed in all three lines, with 1492 genes significantly upregulated and 536 genes downregulated (Figure 7A and [Supplemental Data 1](#)). The differentially expressed genes (DEGs) in GCGT stems were divided into five categories based on their Kyoto Encyclopedia of Genes and Genomes (KEGG) metabolic pathway annotations: cellular processes, environmental information processing, genetic information processing, metabolism, and organismal systems. The branch “metabolism” represented the largest group, in which “carbohydrate metabolism” represented the largest subgroup, followed by “biosynthesis of other secondary

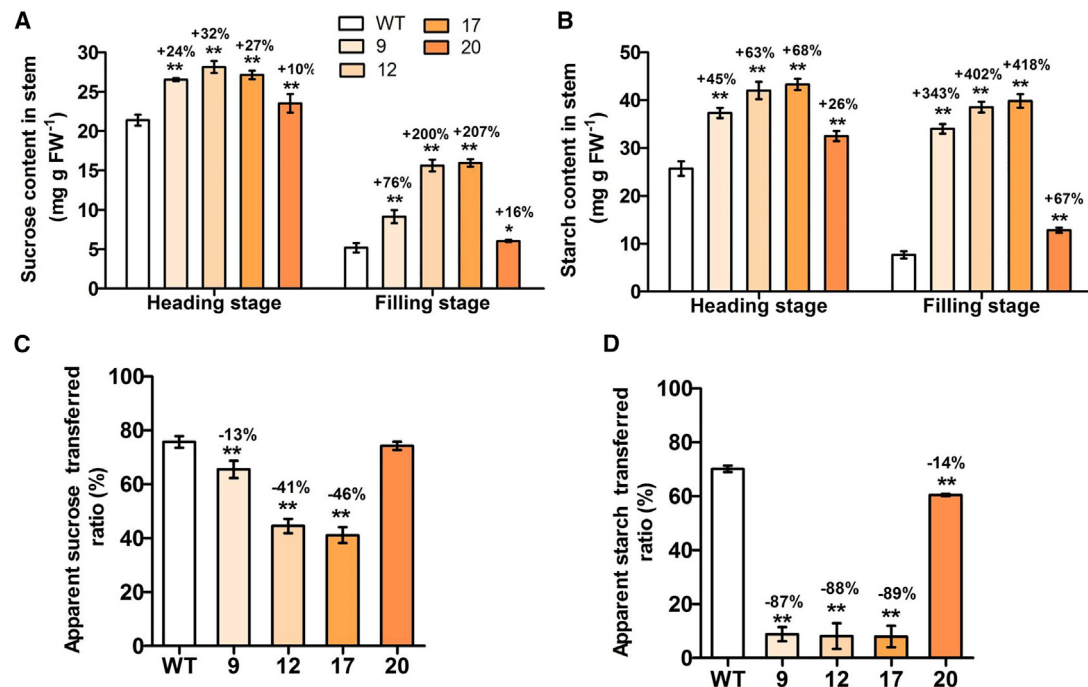


**Figure 6. Carbohydrate Content in the Stems of GCGT Transgenic Plants and the Fraction Transported Out of the Stem.**

(A) The sucrose content in stems (culms and sheaths).

(B) The starch content in stems (culms and sheaths).

(C) The apparent ratio of transferred stem sucrose.

(D) The apparent ratio of transferred stem starch. Data are presented as the mean  $\pm$  SD;  $n = 4$ ; \* $P < 0.05$ ; \*\* $P < 0.01$ , according to one-way ANOVA followed by a Tukey's post hoc test for mean comparisons. ANOVA tables for each analysis are shown in [Supplemental Data 5](#).

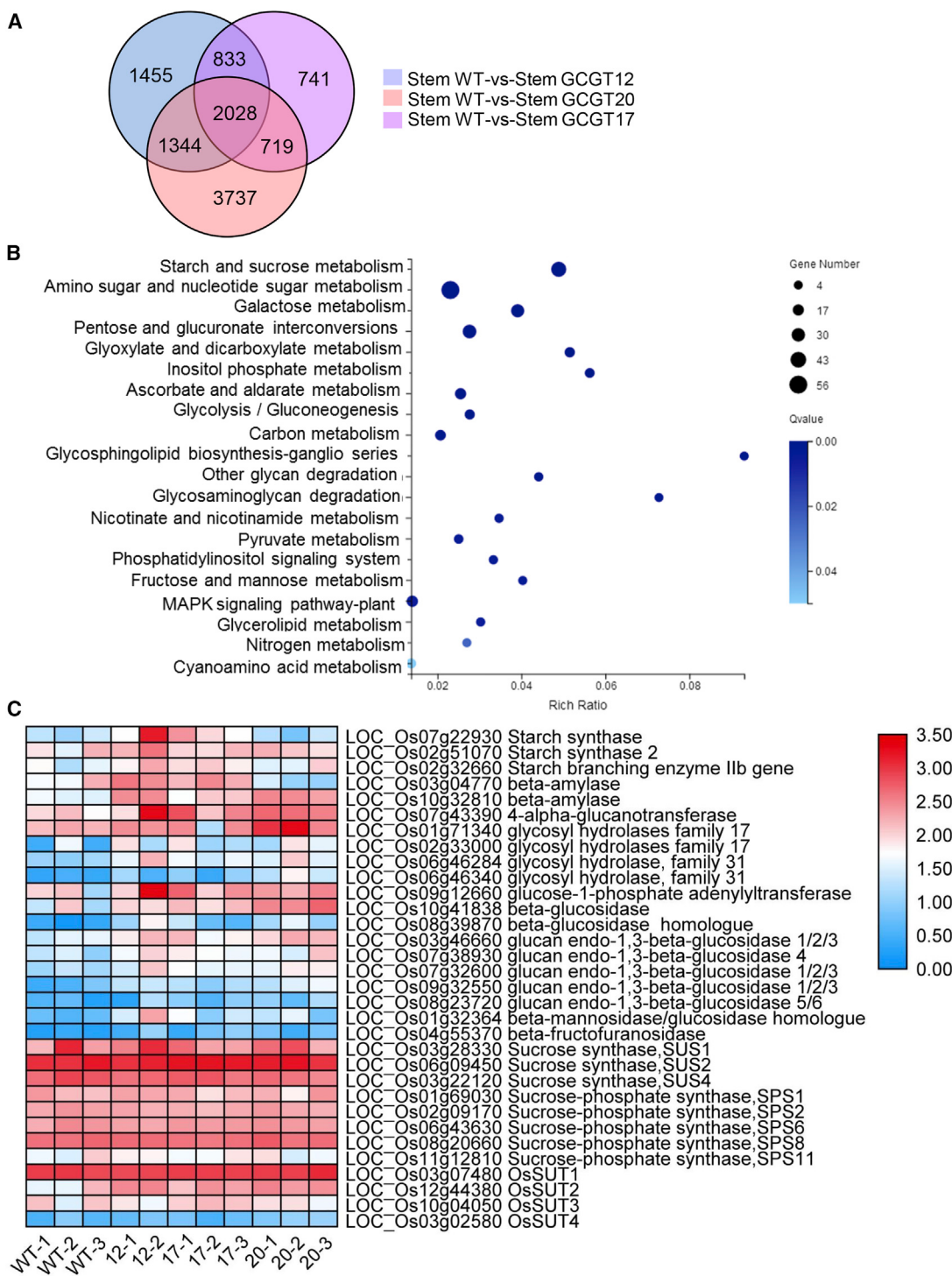
metabolites” ([Supplemental Figure 5](#)). Most of the DEGs involved in carbohydrate metabolism ([Supplemental Figure 6](#) and [Supplemental Data 2](#)) were upregulated. We performed further KEGG pathway enrichment analysis of the DEGs involved in carbohydrate metabolism and observed that the cluster “amino sugar and nucleotide sugar metabolism” represented the largest group, followed by “starch and sucrose metabolism” and “galactose metabolism” ([Figure 7B](#)). Starch is the main non-structural carbohydrate stored in the stems of rice ([Yang et al., 2001](#)), and starch stored in the stems must first be degraded to glucose and then resynthesized into sucrose, which is transported from the stem to the grain for utilization ([Venkateswarlu and Visperas, 1987](#); [Beck and Ziegler, 1989](#); [Yang et al., 2001](#)). Genes that promote starch synthesis and degradation, such as starch synthase, starch branching enzymes,  $\beta$ -amylase, glycosyl hydrolase family enzymes, and  $\beta$ -glucosidase family enzymes, were significantly upregulated in GCGT stems, whereas those involved in photosynthate transportation, such as sucrose-phosphate synthase and sucrose transporters, were not upregulated in GCGT plants ([Figure 7C](#) and [Supplemental Data 3](#)). This may have caused a lack of coordination in source-to-sink flow in GCGT plants, which in turn may have affected the transport of photosynthetic carbohydrates from stems to grains.

## DISCUSSION

The GOC bypass was the first attempt to test a photorespiration bypass in rice. Although increases in photosynthesis and

biomass yield were observed for GOC plants, grain yield varied depending on the seeding season due to different degrees of reduction in seed setting rate ([Shen et al., 2019](#)). Plants with bypass 1 and bypass 3 showed increases in photosynthesis and biomass yield. However, these increases were observed only under low-light and short-day conditions, possibly because the two bypasses ran at low efficiency against the redundancy of NADPH under high-light conditions ([Peterhansel and Maurino, 2011](#); [Peterhansel et al., 2013b](#); [Shen et al., 2019](#)). Therefore, bypass 1 and bypass 3 may not be suitable for rice because it is a high-light species with an LSP greater than  $1600 \mu\text{mol m}^{-2} \text{s}^{-1}$  ([Shen et al., 2019](#)). Other bypasses need to be tested in rice plants to improve seed setting rate and thereby further increase grain yield.

In this study, we successfully established a synthetic photorespiratory shortcut (GCGT bypass) in rice chloroplasts ([Figure 1B](#)), which was different from the bypasses reported previously. In terms of carbon economy, the GCGT bypass can recover 75% of carbon into the Calvin cycle, just like native photorespiration and bypass 1. According to the energy demand calculated by [Peterhansel et al. \(2013a\)](#), 2.5 more ATPs are needed to recycle one glycolate in the GCGT bypass compared with bypass 1, which requires 0.5 less ATP than native photorespiration. Therefore, the advantages of the GCGT bypass may ultimately result from increasing Cc rather than reducing carbon and energy consumption. Compared with the GOC bypass, which completely oxidizes glycolate to CO<sub>2</sub> in chloroplasts without reconnection to the major photorespiratory

**Figure 7. Global Transcriptome Changes in GCGT versus WT Plants.**

(A) Venn diagrams of differentially expressed genes (DEGs) in the stems of GCGT 12, 17, and 20 and WT plants at the filling stage (fold change  $\geq 2.0$ , FDR  $< 0.05$ ).

(B) KEGG pathway enrichment analysis of the DEGs involved in carbohydrate metabolism (fold change  $\geq 2.0$ , FDR  $< 0.05$ ).

(C) Heatmap showing the log fold change in the expression of genes involved in “starch and sucrose metabolism and transportation” between GCGT 12, 17, and 20 versus WT (the fold change compared with control).

pathway, the GCGT bypass recovers 75% of carbon from glycolate metabolism into the Calvin cycle. In addition, the GCGT bypass, which has one  $H_2O_2$ -producing reaction,

produces much less  $H_2O_2$  than the GOC bypass, which has three such reactions. Several lines of evidence indicate that the GCGT bypass functions well in chloroplasts: optimal

expression levels of target genes and high activities of their encoded enzymes (Figure 1C–1G), improved Pn (Figure 3A and 3D), decreased  $\Gamma^*$  (Figure 3E), increased photosynthetic carbohydrate content (Figure 4A and 4B), reduced photorespiration (Figure 5B), and expected changes in photorespiratory metabolites (Figure 5C–5F). More critically, the direct role of this pathway in chloroplastic glycolate metabolism is supported by increased Cc (Figure 5A). In addition, mesophyll cells and chloroplasts in GCGT transgenic plants were significantly larger than those in WT plants (Figure 4C–4H and Supplemental Table 3). Similar phenotypes were noted in bypass 4, bypass 5, and other CO<sub>2</sub>-enriched plants (Wulff and Strain, 1982; Wang et al., 2004; Pritchard et al., 2008; Shen et al., 2019; South et al., 2019). The efficiency of a chloroplastic CO<sub>2</sub> release system strongly depends on the degree of refixation of CO<sub>2</sub> released by mitochondria during photorespiration (Peterhansel et al., 2013a). It has been suggested that the amount of such refixation can be increased if chloroplasts cover the outer surfaces of cells, such that CO<sub>2</sub> released anywhere in the cell must diffuse through chloroplasts to reach the intercellular space (Sage and Sage, 2009). In GCGT transgenic plants, chloroplasts occupied most of the cell space (Figure 4F–4H), and this structural feature reduced the amount of CO<sub>2</sub> lost to the atmosphere. Overall, the flow of carbon through native photorespiration was successfully split, with a portion of the CO<sub>2</sub> released inside chloroplasts. The increased Cc suppressed photorespiration and promoted photosynthesis, ultimately leading to increases in biomass and grain yield. However, other possible mechanisms may also have contributed to increased photosynthesis to a greater or lesser extent. For instance, a significant decrease in glycine level was observed in GCGT plants compared with WT plants, as observed after glycine decarboxylase overexpression in transgenic plants, suggesting that feedback inhibition can be artificially relaxed by decreasing the accumulation of photorespiratory intermediates, particularly at the glycine-to-serine conversion step (Timm et al., 2012).

Rice is a staple food crop, and our objective was to further increase its grain yield. The grain yield performance of GCGT plants was similar to that of GOC plants, which had a lower seed setting rate compared with WT plants and larger decreases observed in the fall than in the spring (Shen et al., 2019). GCGT transgenic plants had higher Pn (Figure 3) and yield compared with WT plants (Figure 2H) but a lower seed setting rate (Figure 2F). Rice grain yield depends on the capacity for assimilation (source), the capacity to utilize the assimilated products in the grain (sink), and the capacity to transport the assimilated products (flow) (Venkateswarlu, 1976; Yang and Zhang, 2010). The source includes two types of carbon, namely assimilates from functional leaves transferred directly to the grain and assimilates redistributed from reserve pools in vegetative tissues (culms and sheaths) at either pre- or post-anthesis (Kobata et al., 1992; Schnyder, 1993; Yang and Zhang, 2010). Photosynthetic efficiency and carbohydrate content were markedly higher in the leaves of GCGT transgenic plants (source) compared with those of WT plants (Figure 4A and 4B), and the main panicle length and grain number per main panicle (sink) were also significantly higher (Figure 2C and 2D), suggesting that both "source" and "sink" were stronger in GCGT plants than in WT plants. Several studies have

demonstrated that remobilization of carbon reserves from the source to the sink (flow) is critical for high grain yields when the source and the sink are not limiting (Palta et al., 1994; Asseng and van Herwaarden, 2003; Plaut et al., 2004). We noticed that the apparent ratios of transferred stem sucrose and starch were significantly lower in the stems of GCGT transgenic plants than in those of WT plants (Figure 6C and 6D). Therefore, we speculate that photosynthetic carbohydrates were not transported to grains at the filling stage in a timely or efficient manner. This is further supported by the RNA-seq analysis.

In the KEGG pathway enrichment analysis of DEGs involved in carbohydrate metabolism in GCGT and WT stems, the cluster "amino sugar and nucleotide sugar metabolism" was the largest group, followed by "starch and sucrose metabolism" (Figure 7B). The differential expression of genes in these functional categories indicated that the conversion of starch to sucrose and the transport of sucrose were affected in GCGT transgenic plants. Starch stored in stems (culms and sheaths) must first be degraded to glucose prior to the re-synthesis of sucrose, which is then transported from stems to grains for utilization (Venkateswarlu and Visperas, 1987; Beck and Ziegler, 1989). Starch degradation can occur through hydrolytic and phosphorolytic reactions (Beck and Ziegler, 1989; Nielsen et al., 1997). Increasing the activities of  $\alpha$ -amylase,  $\beta$ -amylase, and sucrose-phosphate synthase promotes the rapid hydrolysis of starch and the transfer of sucrose from stems to grains (Yang et al., 2001; Wang et al., 2017). Sucrose-phosphate synthase has been shown to play key roles in the re-synthesis of sucrose (Wardlaw and Willenbrink, 1994) and in the maintenance of assimilatory carbon flux from the source to the sink (Isopp et al., 2000). Sucrose loading into the phloem is the first step in long-distance transport from stems to developing grains, and it is mediated by either plasmodesmata or sucrose transporters (Lucas et al., 2013). It has been reported that transgenic rice plants expressing the *Arabidopsis* phloem-specific sucrose transporter AtSUC2 had a 16% increase in grain yield compared with WT plants (Wang et al., 2015). The level of sucrose transporter activity, together with sink demand, essentially determines the amount of carbon that is exported from leaves and stems (Lucas et al., 2013). From our RNA-seq data (Figure 7C), we found that most genes involved in starch synthesis (starch synthase and starch branching enzymes) and degradation ( $\beta$ -amylase, glycosyl hydrolase family enzymes, and  $\beta$ -glucosidase family enzymes) were highly upregulated in GCGT transgenic plants, but sucrose-phosphate synthase and sucrose transporters were not. This lack of coordination may be the reason for the above-mentioned "traffic jam" of photosynthates, which reduced the seed setting rate in GCGT plants.

More interestingly, the seed setting rate was found to decrease further as the photosynthetic efficiency increased. For instance, GCGT 20 plants showed the highest increase in yield compared with WT plants but had the lowest increase in Pn, which increased by only 6%. By contrast, Pn increased by 10%–16% in the other three lines (Figures 2H and 3D). GCGT 20 plants also accumulated the least amount of sucrose and starch in stems (Figure 6A and 6B), so that the apparent ratios of transferred stem sucrose and starch for GCGT 20 plants were significantly higher than those for the other GCGT lines (Figure 6C and 6D). GCGT 20 plants also had a higher seed setting rate and the

greatest increase in grain yield (Figure 2F and 2H). Thus, it seems that a moderate increase in photosynthesis is more beneficial for increasing rice grain yield. Based on the similar reduced seed setting rate observed for both the GOC and GGCT plants, we may conclude that increases in grain yield may not necessarily correlate with increases in biomass yield, contrary to the opinion of South et al. (2019). Although the enhancement of photosynthetic efficiency is viewed as the most promising way to further increase crop yields in the future—and the ability of synthetic photorespiratory bypasses (either circuit or open types) to improve photosynthesis and biomass yield has been well documented (this study, Kebeish et al., 2007; Maier et al., 2012; Nölke et al., 2014; Dalal et al., 2015; South et al., 2019; Shen et al., 2019)—the coordinated transport of photosynthetic carbohydrates during grain filling should receive additional consideration. As long as the ultimate objective is to increase crop grain yield, then carbohydrate transport may be a key point of leverage for resolving the divergence between photosynthesis and grain yield, as the view is still held that increasing photosynthesis is unlikely to increase crop yields (Sinclair et al., 2019). Molecular and genetic improvements in the transport process are clearly needed to finally solve the seed setting rate problem based on an understanding of how increased photosynthesis causes a photosynthate traffic jam. We are using other, easier approaches, including (1) transforming different rice varieties that differ in stem non-structural carbohydrate translocation and grain filling characteristics (Li et al., 2017); (2) replacing the currently used constitutive promoters with light- and mesophyll-specific promoters or drought-inducible promoters, aiming for better coordination between source and transport capacities (Chen et al., 2020); and (3) transforming different tuberous crops, such as potato, sweet potato, and cassava, as unlike cereal grains, the tuber is a vegetative organ which requires no grain filling.

## METHODS

### Construction of the GCGT-pYL1305 Multi-Gene Expression Vector and Genetic Transformation into Rice

The GCGT-pYL1305 multi-gene expression vector was constructed as described by Shen et al. (2019) with minor modifications. DNA sequences of *OsGLO1* (*Os03g0786100*), *EcCAT* (*WP\_000077872.1*), *EcGCL* (*WP\_061352092.1*), and *EcTSR* (*WP\_021571777.1*) were amplified by PCR, with the *in situ* peroxisomal targeting sequence of *OsGLO1* replaced by the 6×His-tagged sequence. *EcGCL* and *EcTSR* were fused by a (Gly3Ser)3 linker sequence (Nölke et al., 2014), and the 6×His-tagged sequence was fused to the 5' end of *EcGCL*. The structure of *EcGCL\*TSR* is shown in Supplemental Figure 1. The rCTP sequence was fused to the 5' end of *OsGL O 1*, and the modified rCTP (RC2) sequence was then fused to the 5' end of *EcCAT* and *EcGCL\*TSR* by digesting with the appropriate restriction enzyme (Shen et al., 2017). The sequences of *rCTP-OsGLO1*, *RC2-EcCAT*, and *RC2-EcGCL\*TSR* fusion genes are listed in Supplemental Data 4. Using previously described Cre/loxP homologous recombination technology (Zhu et al., 2017, 2018), *RC2-EcCAT* and *RC2-EcGCL\*TSR* fusion genes were introduced into  *pYL322d1*, and the *rCTP-OsGLO1* fusion gene was introduced into *pYL322d2* and then assembled into the multi-gene expression vector *pYL1305*. The multi-gene expression vector GCGT-pYL1305 containing the four target genes, *OsGLO1*, *EcCAT*, *EcGCL*, and *EcTSR*, was constructed; expression of *EcCAT* and *EcGCL\*TSR* was driven by *pUBi*, and that of *OsGLO1* was driven by *pE35S*. The structure of GCGT-pYL1305 is shown in Figure 1A. *pYL322d1*, *pYL322d2*, and *pYL1305* vectors were kindly provided by Dr. Yao-Guang Liu, College of

### Photorespiratory Shortcut Enhances Photosynthesis

Life Sciences, South China Agricultural University. The constructed vector GCGT-pYL1305 was transformed into rice (*O. sativa L. cv. Zhonghua11*) via *Agrobacterium*-mediated infection (strain EHA105). Homozygous lines were obtained by screening for hygromycin resistance.

### Plant Growth Conditions

The experiments were carried out on an experimental farm on the campus of the South China Agricultural University, Guangzhou, China. Rice plants (cv. Zhonghua11) were used as the WT experimental material. The four GCGT lines (GCGT 9, 12, 17, and 20) were homozygous for the transgene. After germination on moist filter paper for 36–48 h, the seeds were grown in Kimura B complete nutrient solution (Yoshida et al., 1971) in a glasshouse with a PFD of 800–1000  $\mu\text{mol m}^{-2} \text{s}^{-1}$ , a light/dark cycle of 14 h/10 h, a temperature of 25°C–30°C, and relative humidity of 60%–80% for 21 days and then transplanted to pots or paddy fields for further growth. For the pot experiments, each pot contained one WT (Zhonghua11) seedling and three GCGT seedlings, each from a separate line. For the field experiments, the WT and four GCGT lines were arranged in a randomized block design with six replicates under natural conditions with a planting density of 25 × 25 cm per plant. Each plot area was approximately 16 m<sup>2</sup> (4 × 4 m). The pot experiments were conducted in 2018 and 2019. The field experiments were conducted in 2019.

### Gene Expression, Protein Detection, and Enzyme Assays

Total RNA was extracted from rice leaves using TRIzol reagent (Life Technologies, USA), and first-strand cDNA was synthesized using ReverTra Ace (Toyobo, Japan). The primers for RT-PCR are listed in Supplemental Table 1. Proteins were extracted as described by Shen et al. (2019). Fresh leaves (100 mg) were homogenized in 1 ml of 0.1 M phosphate buffer (pH 8.0) and centrifuged at 12 000 rpm for 15 min at 4°C to remove cell debris. Equal amounts of protein were loaded and separated by SDS-PAGE, and proteins were transferred onto polyvinylidene fluoride membranes. *OsGLO1*, *EcCAT*, and *EcGCL\*TSR* proteins were detected using a monoclonal anti-His antibody (Abmart, USA). An alkaline phosphatase-linked antibody (Abmart) was used as the secondary antibody, and staining of the large subunit of Rubisco with Ponceau S served as the control.

GLO and CAT activities were determined as described previously by Shen et al. (2019), whereas GCL and TSR activities were assayed in a coupled reaction (Goto and Kornberg, 1961; Kebeish et al., 2007).

### Gas-Exchange Measurements and Chlorophyll Fluorescence Analysis

An open flow gas exchange system (LI-6800, LI-COR, USA) was used to measure leaf gas exchange in the newest fully expanded flag leaf at the filling stage. Diurnal Pn curves, light response curves, and CO<sub>2</sub> response curves were constructed as described previously by Shen et al. (2019). The light response and CO<sub>2</sub> response curves were fitted using the LI-COR software for calculating AQE, A<sub>max</sub>, and LSP. The photorespiration rate was estimated according to Yeo et al. (1994). The photorespiration rate was calculated as the difference between Pn under low (2% O<sub>2</sub>) and normal (21% O<sub>2</sub>) oxygen conditions. Chlorophyll fluorescence was measured using a gas exchange system (LI-6800, LI-COR, USA) with a fluorescence leaf chamber. Leaves were dark-adapted for at least 20 min before the measurement of F<sub>v</sub>/F<sub>m</sub>. The variable J method described by Harley et al. (1992) was used to calculate Cc as follows:

$$Cc = \frac{\Gamma^*(J + 8(A + Rd))}{J - 4(A + Rd)}.$$

$\Gamma^*$  and day respiration (R<sub>d</sub>) were determined using the Laisk method described by Shen et al. (2019), and the curves were analyzed using the linearization method of Walker et al. (2016b). In brief, the linear portion of the CO<sub>2</sub> response curves (CO<sub>2</sub> concentrations from 100 to

## Photorespiratory Shortcut Enhances Photosynthesis

20  $\mu\text{mol mol}^{-1}$  was measured under three different PFDs (100, 300, and 600  $\mu\text{mol m}^{-2} \text{s}^{-1}$ ) with a gas exchange system, and linear regression lines were fitted to the responses for each PFD. The intersection point of the three  $\text{CO}_2$  response curves was considered to be  $\Gamma^*$  (x axis) and  $R_d$  (y axis).

### Preparation of Ultrathin Sections of Rice Leaves and Ultrastructure Observation

Ultrathin sections were prepared as described previously by Shen et al. (2019) with minor modifications. The leaves and leaf sheaths of GCGT transgenic and WT plants at the filling stage were cut into squares (1 mm<sup>3</sup>), prefixed in Karnovsky's fixative (3% paraformaldehyde and 4% glutaraldehyde in 0.1 M phosphate buffer [pH 7.2]) for at least 24 h at 4°C, washed five times in 0.1 M phosphate buffer (pH 7.2) for 15 min, post-fixed in 1% OsO<sub>4</sub> for 2 h at room temperature, and washed five times in 0.1 M phosphate buffer (pH 7.2) for 10 min. After gradient dehydration in a series of alcohol and acetone baths, the samples were immersed in 50% Epon 812 epoxy resin for 24 h, followed by 70% epoxy resin for 24 h, and then 100% epoxy resin for 24 h before polymerization at 40°C for 24 h and 60°C for 48 h. Ultrathin sections (70–80 nm) were prepared using a diamond knife, stained with uranyl acetate for 20 min, and counterstained with lead citrate for 10 min. The sections were observed and photographed using a Philip FEI Tecnai 12 transmission electron microscope.

### Measurement of Sucrose, Starch, and Metabolite Contents

For sucrose and starch measurement, flag leaves and stems (culms and sheaths) were sampled separately from 14:00 to 14:30 h and oven-dried at 80°C to constant weight. Dried flag leaves and stems (culms and sheaths) were ground to a powder using a pulverizer. The sample powder (0.5 g) was extracted three times with 80% ethanol at 80°C for 30 min. After centrifugation at 5000 g for 15 min, the supernatant was used to measure the sucrose content, and the pellets were used to measure the starch content. The sucrose content was measured according to Luo and Huang (2011), whereas the starch content was measured according to Nakamura and Miyachi (1982). The apparent ratios of transferred stem sucrose and starch were calculated as described by Li et al. (2017) with minor modifications as follows: apparent ratio of transferred stem sucrose (%) = [(sucrose content in stems and sheaths at heading stage – sucrose content in stems and sheaths at filling stage)/sucrose content in stems and sheaths at heading stage] × 100%; apparent ratio of transferred stem starch (%) = [(starch content in stems and sheaths at heading stage – starch content in stems and sheaths at filling stage)/starch content in stems and sheaths at heading stage] × 100%.

For the analysis of other metabolites, flag leaves were detached from plants at 14:00 to 14.30 h, and the detached leaves were quickly frozen in liquid nitrogen. For analysis, leaf material was homogenized in liquid nitrogen immediately extracted in 70% ice-cold methanol, and subjected to GC-MS as described in Liseć et al. (2006).

### RNA-Seq Analysis

The RNA-seq analysis was conducted using total RNA extracted from stems (culms and sheaths) of three GCGT lines (GCGT 12, 17, and 20) and the WT at the filling stage with three biological replicates. Total RNA was extracted using TRIzol reagent. Oligo (dT)-attached magnetic beads were used to purify the mRNA. RNA-seq analysis was performed using the BGISEQ-500 platform at BGI (Wuhan, China).

The sequencing data were filtered using SOAPnuke (v1.5.2) (<https://github.com/BGI-flexlab/SOAPnuke>). The resulting clean reads were stored in FASTQ format and mapped to the reference genome using HISAT2 (v2.0.4) (<http://www.ccb.jhu.edu/software/hisat/index.shtml>). Differential expression analysis was performed using DESeq2 (v1.4.5) (<http://www.bioconductor.org/packages/release/bioc/html/DESeq2.html>) with a Q-value threshold of  $\leq 0.05$ . To gain insight into phenotypic changes, Gene Ontology (<http://www.geneontology.org/>) and KEGG (<https://www.kegg.jp/>) enrichment analysis of annotated DEGs was performed using phyper in R based on the hypergeometric test ([https://en.wikipedia.org/wiki/Hypergeometric\\_distribution](https://en.wikipedia.org/wiki/Hypergeometric_distribution)).

## Molecular Plant

The fragment counts for each gene were normalized by kb of transcript per million mapped reads to obtain the fragments per kilobase of exon model per million mapped reads. Differential expression analysis of treatments versus controls was performed using the cuffdiff program, and significant DEGs used for further data analysis were filtered based on a false discovery rate (FDR)-corrected *P*-value of  $<0.05$  and a fold change of  $\geq 2$ . The DEGs in the stems of GCGT transgenic plants (GCGT 12, 17, and 20) and the WT are listed in *Supplemental Data 1*.

### Statistical Analysis

Significance was evaluated by one-way analysis of variance (ANOVA). All ANOVAs were followed by a Tukey's *post hoc* test for mean comparison using SPSS software (v19.0, IBM, USA). ANOVA tables for each analysis are shown in *Supplemental Data 5*.

### SUPPLEMENTAL INFORMATION

Supplemental Information can be found online at *Molecular Plant Online*.

### FUNDING

This work was supported by the Major Program of Guangdong Basic and Applied Research (2019B030302006) and the National Key Research and Development Program (2020YFA0907600), China.

### AUTHOR CONTRIBUTIONS

X.-X.P., L.-M.W., and B.-R.S. conceived and designed the experiments. L.-M.W., B.-R.S., B.-D.L., C.-L.Z., M.L., P.-P.T., L.-L.C., and Z.-S.Z. performed the experiments. L.-M.W. and B.-R.S. analyzed the data. X.-X.P. and L.-M.W. wrote the paper. X.-X.P. revised and approved the final version of the paper.

### ACKNOWLEDGMENTS

We thank Dr. Yaoguang Liu (College of Life Sciences, South China Agricultural University) for providing the multi-gene expression vectors. No conflict of interest declared.

Received: June 2, 2020

Revised: September 16, 2020

Accepted: October 14, 2020

Published: October 16, 2020

### REFERENCES

- Asseng, S., and van Herwaarden, A.F. (2003). Analysis of the benefits to wheat yield from assimilates stored prior to grain filling in a range of environments. *Plant Soil* **256**:217–219.
- Bauwe, H., Hagemann, M., and Fernie, A.R. (2010). Photorespiration: players, partners and origin. *Trends Plant Sci.* **15**:330–336.
- Beck, A., and Ziegler, P. (1989). Biosynthesis and degradation of starch in higher plants. *Annu. Rev. Plant Physiol. Plant Mol. Biol.* **40**:95–117.
- Berry, J.A., Osmond, C.B., and Lorimer, G.H. (1978). Fixation of O<sub>2</sub> during photorespiration: kinetic and steady-state studies of the photorespiratory carbon oxidation cycle with intact leaves and isolated chloroplasts of C(3) plants. *Plant Physiol.* **62**:954–967.
- Betti, M., Bauwe, H., Busch, F.A., Fernie, A.R., Keech, O., Levey, M., Ort, D.R., Parry, M.A.J., Sage, R., Timm, S., et al. (2016). Manipulating photorespiration to increase plant productivity: recent advances and perspectives for crop improvement. *J. Exp. Bot.* **67**:2977–2988.
- Carvalho, Jde F., Madgwick, P.J., Powers, S.J., Keys, A.J., Lea, P.J., and Parry, M.A. (2011). An engineered pathway for glyoxylate

## Molecular Plant

- metabolism in tobacco plants aimed to avoid the release of ammonia in photorespiration. *BMC Biotechnol.* **11**:111.
- Chen, J., Chen, S., He, N., Wang, Q., Zhao, Y., Gao, W., and Guo, F.** (2020). Nuclear-encoded synthesis of the D1 subunit of photosystem II increases photosynthetic efficiency and crop yield. *Nat. Plants* **6**:570–580.
- Dalal, J., Lopez, H., Vasani, N.B., Hu, Z., Swift, J.E., Yalamanchili, R., Dvora, M., Lin, X., Xie, D., and Qu, R.** (2015). A photorespiratory bypass increases plant growth and seed yield in biofuel crop *Camelina sativa*. *Biotechnol. Biofuels* **8**:175.
- Gotto, A.M., and Kornberg, H.L.** (1961). The metabolism of C<sub>2</sub> compounds in micro-organisms. 7. Preparation and properties of crystalline tartronic semialdehyde reductase. *Biochem. J.* **81**:273–284.
- Harley, P.C., Loreto, F., Di Marco, G., and Sharkey, T.D.** (1992). Theoretical considerations when estimating the mesophyll conductance to CO<sub>2</sub> flux by analysis of the response of photosynthesis to CO<sub>2</sub>. *Plant Physiol.* **98**:1429–1436.
- Heyneke, E., and Fernie, A.R.** (2018). Metabolic regulation of photosynthesis. *Biochem. Soc. Trans.* **46**:321–328.
- Isopp, H., Frehner, M., Long, S.P., and Nosberger, J.** (2000). Sucrose-phosphate synthase responds differently to source-sink relation and photosynthetic rates: *Lolium perenne* L. growing at elevated Pco<sub>2</sub> in the field. *Plant Cell Environ.* **23**:597–607.
- Kebeish, R., Niessen, M., Thiruveedhi, K., Bari, R., Hirsch, H., Rosenkranz, R., Stäbler, N., Schönfeld, B., Kreuzaler, F., and Peterhänsel, C.** (2007). Chloroplastic photorespiratory bypass increases photosynthesis and biomass production in *Arabidopsis thaliana*. *Nat. Biotechnol.* **25**:593–599.
- Kobata, T., Palta, J.A., and Turner, N.C.** (1992). Rate of development of postanthesis water deficits and grain filling of spring wheat. *Crop Sci.* **32**:1238–1242.
- Li, G., Pan, J., Cui, K., Yuan, M., Hu, Q., Wang, W., Mohapatra, P., Nie, L., Huang, J., and Peng, S.** (2017). Limitation of unloading in the developing grains is a possible cause responsible for low stem non-structural carbohydrate translocation and poor grain yield formation in rice through verification of recombinant inbred lines. *Front. Plant Sci.* **8**:1369.
- Liu, J., Cui, L., Xie, Z., Zhang, Z., Liu, E., and Peng, X.** (2019). Two NCA1 isoforms interact with catalase in a mutually exclusive manner to redundantly regulate its activity in rice. *BMC Plant Biol.* **19**:105.
- Lisec, J., Schauer, N., Kopka, J., Willmitzer, L., and Fernie, A.R.** (2006). Gas chromatography mass spectrometry-based metabolite profiling in plants. *Nat. Protoc.* **1**:387.
- Long, S.P., Ainsworth, E.A., Leakey, A.D., Nösberger, J., and Ort, D.R.** (2006). Food for thought: lower-than-expected crop yield stimulation with rising CO<sub>2</sub> concentrations. *Science* **312**:1918–1921.
- Long, S.P., Marshall-Colon, A., and Zhu, X.** (2015). Meeting the global food demand of the future by engineering crop photosynthesis and yield potential. *Cell* **161**:56–66.
- Lucas, W.J., Groover, A., Lichtenberger, R., Furuta, K., Yadav, S.R., Helariutta, Y., He, X., Fukuda, H., Kang, J., and Brady, S.M.** (2013). The plant vascular system: evolution, development and functions. *J. Integr. Plant Biol.* **55**:294–388.
- Luo, X., and Huang, Q.** (2011). Relationships between leaf and stem soluble sugar content and tuberous root starch accumulation in Cassava. *J. Agric. Sci.* **3**:64–72.
- Maier, A., Fahnstich, H., von Caemmerer, S., Engqvist, M.K.M., Weber, A.P.M., Flügge, U., and Maurino, V.G.** (2012). Transgenic introduction of a glycolate oxidative cycle into *A. thaliana* chloroplasts leads to growth improvement. *Front. Plant Sci.* **3**:1–12.
- Photorespiratory Shortcut Enhances Photosynthesis**
- Nakamura, Y., and Miyachi, S.** (1982). Effect of temperature on starch degradation in *Chlorella vulgaris* 11 h cells. *Plant Cell Physiol.* **23**:333–341.
- Nielsen, T.H., Deiting, U., and Stitt, M.** (1997). A [beta]-amylase in potato tubers is induced by storage at low temperature. *Plant Physiol.* **113**:503–510.
- Nölke, G., Houdelet, M., Kreuzaler, F., Peterhänsel, C., and Schillberg, S.** (2014). The expression of a recombinant glycolate dehydrogenase polyprotein in potato (*Solanum tuberosum*) plastids strongly enhances photosynthesis and tuber yield. *Plant Biotechnol. J.* **12**:734–742.
- Novitskaya, L., Trevanion, S.J., Driscoll, S., Foyer, C.H., and Noctor, G.** (2002). How does photorespiration modulate leaf amino acid contents? A dual approach through modelling and metabolite analysis. *Plant Cell Environ.* **25**:821–835.
- Palta, J.A., Kobata, T., Turner, N.C., and Fillery, I.R.** (1994). Remobilization of carbon and nitrogen in wheat as influenced by post-anthesis water deficits. *Crop Sci.* **34**:118–124.
- Peterhansel, C., Blume, C., and Offermann, S.** (2013a). Photorespiratory bypasses: how can they work? *J. Exp. Bot.* **64**:709–715.
- Peterhansel, C., Horst, I., Niessen, M., Blume, C., Kebeish, R., Kürkcüoglu, S., and Kreuzaler, F.** (2010). Photorespiration. *Arabidopsis Book*. **8**:e0130.
- Peterhansel, C., Krause, K., Braun, H.P., Espie, G.S., Fernie, A.R., Hanson, D.T., Keech, O., Maurino, V.G., Mielewczik, M., and Sage, R.F.** (2013b). Engineering photorespiration: current state and future possibilities. *Plant Biol.* **15**:754.
- Peterhansel, C., and Maurino, V.G.** (2011). Photorespiration redesigned. *Plant Physiol.* **155**:49–55.
- Plaut, Z., Butow, B.J., Blumenthal, C.S., and Wrigley, C.W.** (2004). Transport of dry matter into developing wheat kernels and its contribution to grain yield under post-anthesis water deficit and elevated temperature. *Field Crops Res.* **86**:185–198.
- Pritchard, S.G., Peterson, C.M., Prior, S.A., and Rogers, H.H.** (2008). Elevated atmospheric CO<sub>2</sub> differentially affects needle chloroplast ultrastructure and phloem anatomy in *Pinus palustris*: interaction with soil resource availability. *Plant Cell Environ.* **20**:461–471.
- Ray, D.K., Mueller, N.D., West, P.C., Foley, J.A., and Hart, J.P.** (2013). Yield trends are insufficient to double global crop production by 2050. *PLoS One* **8**:e66428.
- Sage, T.L., and Sage, R.F.** (2009). The functional anatomy of rice leaves: implications for refixation of photorespiratory CO<sub>2</sub> and efforts to engineer C<sub>4</sub> photosynthesis into rice. *Plant Cell Physiol.* **50**:756–772.
- Schnyder, H.** (1993). The role of carbohydrate storage and redistribution in the source-sink relations of wheat and barley during grain filling—a review. *New Phytol.* **123**:233–245.
- Scofield, G.N., Ruuska, S.A., Aoki, N., Lewis, D.C., Tabe, L.M., and Jenkins, C.L.D.** (2009). Starch storage in the stems of wheat plants: localization and temporal changes. *Ann. Bot.* **103**:859–868.
- Shen, B., Wang, L., Lin, X., Yao, Z., Xue, H., Zhu, C., Teng, H., Cui, L., Liu, E., Zhang, J., et al.** (2019). Engineering a new chloroplastic photorespiratory bypass to increase photosynthetic efficiency and productivity in rice. *Mol. Plant* **2**:199–214.
- Shen, B., Zhu, C., Yao, Z., Cui, L., Zhang, J., Yang, C., He, Z., and Peng, X.** (2017). An optimized transit peptide for effective targeting of diverse foreign proteins into chloroplasts in rice. *Sci. Rep.* **7**:46231.
- Sinclair, T.R., Rufty, T.W., and Lewis, R.S.** (2019). Increasing photosynthesis: unlikely solution for world food problem. *Trends Plant Sci.* **24**:1032–1039.

## Photorespiratory Shortcut Enhances Photosynthesis

## Molecular Plant

- Somerville, R.C.** (2001). An early *Arabidopsis* demonstration: resolving a few issues concerning photorespiration. *Plant Physiol.* **125**:20–24.
- South, P.F., Cavanagh, A.P., Liu, H., and Ort, D.R.** (2019). Synthetic glycolate metabolism pathways stimulate crop growth and productivity in the field. *Science* **363**:t9077.
- South, P.F., Cavanagh, A.P., Lopez-Calcagno, P.E., Raines, C.A., and Ort, D.R.** (2018). Optimizing photorespiration for improved crop productivity. *J. Integr. Plant Biol.* **60**:1217–1230.
- Tilman, D., Balzer, C., Hill, J., and Befort, B.L.** (2011). Global food demand and the sustainable intensification of agriculture. *Proc. Natl. Acad. Sci. U S A* **108**:20260–20264.
- Timm, T., Florian, A., Arrivault, S., Stitt, M., Fernie, A.R., and Bauwe, H.** (2012). Glycine decarboxylase controls photosynthesis and plant growth. *FEBS Lett.* **586**:3692–3697.
- Venkateswarlu, B.** (1976). Source-sink interrelationships in lowland rice. *Plant Soil* **44**:575–586.
- Venkateswarlu, B., and Visperas, R.M.** (1987). Source-sink relationships in crop plants. *IRRI Res. Paper* **125**:19–21.
- Von Caemmerer, S., Quick, W.P., and Furbank, R.T.** (2012). The development of C4 rice: current progress and future challenges. *Science* **336**:1671–1672.
- Walker, B.J., Skabelund, D.C., Busch, F.A., and Ort, D.R.** (2016b). An improved approach for measuring the impact of multiple CO<sub>2</sub> conductances on the apparent photorespiratory CO<sub>2</sub> compensation point through slope-intercept regression. *Plant Cell Environ.* **39**:1198–1203.
- Walker, B.J., VanLoocke, A., Bernacchi, C.J., and Ort, D.R.** (2016a). The costs of photorespiration to food production now and in the future. *Annu. Rev. Plant Biol.* **67**:107.
- Wang, G., Hao, S., Gao, B., Chen, M., Liu, Y., Yang, J., Ye, N., and Zhang, J.** (2017). Regulation of gene expressions in the remobilization of carbon reserve in straws of rice at grain filling. *Plant Cell Physiol.* **58**:1391–1404.
- Wang, L., Lu, Q., Wen, X., and Lu, C.** (2015). Enhanced sucrose loading improves rice yield by increasing grain size. *Plant Physiol.* **169**:2848–2862.
- Wang, X., Anderson, O.R., and Griffin, K.L.** (2004). Chloroplast numbers, mitochondrion numbers and carbon assimilation physiology of *Nicotiana sylvestris* as affected by CO<sub>2</sub> concentration. *Environ. Exp. Bot.* **51**:21–31.
- Wardlaw, I.F., and Willenbrink, J.** (1994). Carbohydrate storage and mobilization by the culm of wheat between heading and grain maturity: the relation to sucrose synthase and sucrose-phosphate synthase. *Austrian J. Plant Physiol.* **21**:255–271.
- Wingler, A., Lea, P.J., Quick, W.P., and Leegood, R.C.** (2000). Photorespiration: metabolic pathways and their role in stress protection. *Philos. Trans. R. Soc. Lond.* **355**:1517–1529.
- Wulff, R.D., and Strain, B.R.** (1982). Effects of CO<sub>2</sub> enrichment on growth and photosynthesis in *Desmodium paniculatum*. *Can. J. Bot.* **60**:1084–1091.
- Yang, J., and Zhang, J.** (2010). Grain-filling problem in 'super' rice. *J. Exp. Bot.* **61**:1–5.
- Yang, J., Zhang, J., Wang, Z., and Zhu, Q.** (2001). Activities of starch hydrolytic enzymes and sucrose-phosphate synthase in the stems of rice subjected to water stress during grain filling. *J. Exp. Bot.* **52**:2169–2179.
- Yeo, M.E., Yeo, A.R., and Flowers, T.J.** (1994). Photosynthesis and photorespiration in the genus *Oryza*. *J. Exp. Bot.* **45**:553–560.
- Yoshida, S., Forno, D.A., and Cock, J.H.** (1971). Laboratory Manual for Physiological Studies of Rice (Manila: International Rice Research Institute).
- Zhang, Z., Lu, Y., Zhai, L., Deng, R., Jiang, J., Li, Y., He, Z., and Peng, X.** (2012). Glycolate oxidase isozymes are coordinately controlled by GLO1 and GLO4 in rice. *PLoS One* **7**:e39658.
- Zhu, Q., Yu, S., Zeng, D., Liu, H., Wang, H., Yang, Z., Xie, X., Shen, R., Tan, J., Li, H., et al.** (2017). Development of "purple endosperm rice" by engineering anthocyanin biosynthesis in the endosperm with a high-efficiency transgene stacking system. *Mol. Plant* **10**:918–929.
- Zhu, Q., Zeng, D., Yu, S., Cui, C., Li, J., Li, H., Chen, J., Zhang, R., Zhao, X., Chen, L., et al.** (2018). From golden rice to aSTARice: bioengineering astaxanthin biosynthesis in rice endosperm. *Mol. Plant* **11**:1440–1448.
- Zhu, X., Long, S.P., and Ort, D.R.** (2008). What is the maximum efficiency with which photosynthesis can convert solar energy into biomass? *Curr. Opin. Biotechnol.* **19**:153–159.

**Supplemental Information**

**A Synthetic Photorespiratory Shortcut Enhances Photosynthesis to Boost Biomass and Grain Yield in Rice**

**Li-Min Wang, Bo-Ran Shen, Bo-Di Li, Chuan-Ling Zhang, Min Lin, Pan-Pan Tong, Li-Li Cui, Zhi-Sheng Zhang, and Xin-Xiang Peng**

1    **Supplemental Data**

2    Supplemental Figure 1. Structure of GCL\*TSR Fusion Protein.

3    Supplemental Figure 2. Kinetic Parameters of GCL\*TSR, GCL, and TSR.

4    Supplemental Figure 3. Glucose and Fructose Contents of GCGT Transgenic Plants at the Filling  
5    Stage.

6    Supplemental Figure 4. Electron Micrographs of Leaf Sheaths of GCGT Transgenic Plants at the  
7    Filling Stage.

8    Supplemental Figure 5. KEGG Pathway Annotation Classification in the Stems of GCGT 12, 17, and  
9    20 versus WT Plants at the Filling Stage.

10   Supplemental Figure 6. Heatmap Showing the Log Fold Change in the Expression of DEGs Involved  
11   in “Carbohydrate Metabolism” in the Stems between GCGT 12, 17, and 20 vs. WT at the Filling  
12   Stage.

13

14   Supplemental Table 1. Primers Used for RT-PCR

15   Supplemental Table 2. Gas Exchange and Chlorophyll Fluorescence Parameters of GCGT and WT  
16   Plants

17   Supplemental Table 3. Sizes and Numbers of Mesophyll Cells and Chloroplasts of GCGT and WT  
18   Plants at the Filling Stage

19

20

21

22

23

24

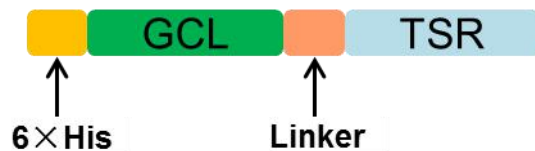
25

26

27

28    **Supplemental Figure 1**

29



31    **Supplemental Figure 1. Structure of GCL\*TSR Fusion Protein.**

32    The (Gly3Ser)3 linker was used to link GCL and TSR. The His tag was added to the N-terminus of  
33    the fusion protein.

34

35

36

37

38

39

40

41

42

43

44

45

46

47

48

49

50

51

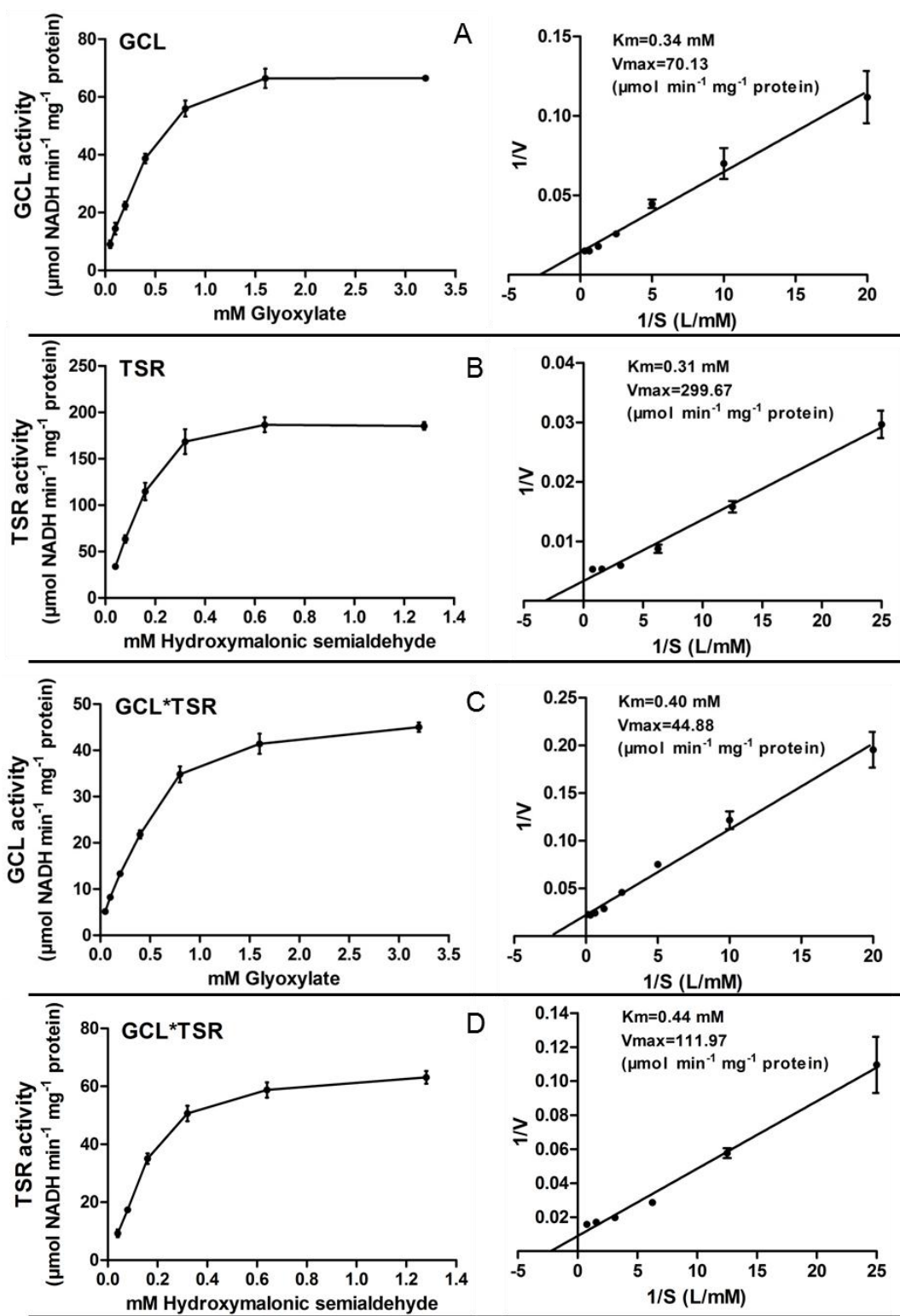
52

53

54

55 **Supplemental Figure 2**

56



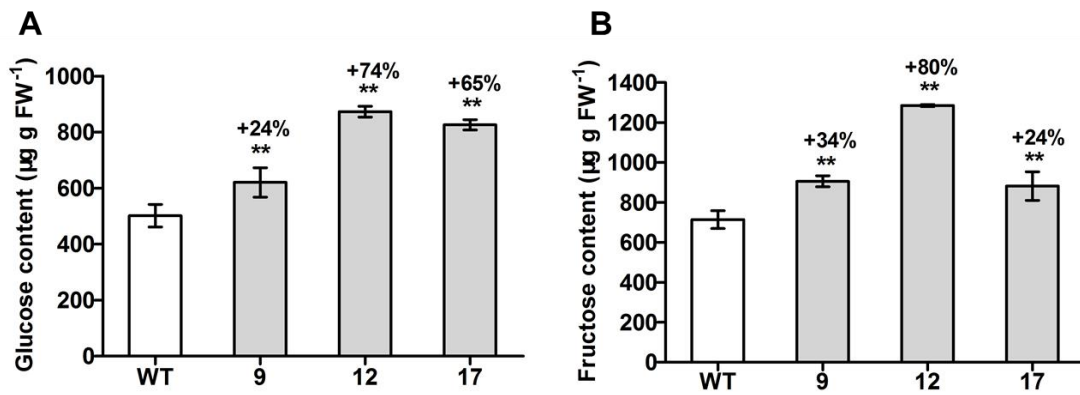
57

58 **Supplemental Figure 2. Kinetic Parameters of GCL, TSR, and GCL\*TSR.**

59 **(A)** GCL activity and  $K_m$ . **(B)** TSR activity and  $K_m$ . **(C)** GCL activity and  $K_m$  of GCL\*TSR. **(D)** TSR  
 60 activity and  $K_m$  of GCL\*TSR. GCL\*TSR: GCL, and TSR fusion protein. Measurements were  
 61 conducted in PBS buffer (pH 8.0) at 37°C.

62 **Supplemental Figure 3**

63

64  
65 **Supplemental Figure 3. Glucose and Fructose Contents of GCGT Transgenic Plants at the  
66 Filling Stage.**67 (A) Glucose content. (B) Fructose content. Metabolite levels (relative to the internal standard ribitol)  
68 were measured by GC-MS using samples harvested at 14:00-14:30 (photorespiratory conditions),  
69  $n=4$ . Data are presented as the mean  $\pm$  SD, \*,  $P < 0.05$ ; \*\*,  $P < 0.01$ , according to one-way ANOVA,  
70 followed with a Tukey's posthoc test for means comparison. ANOVA tables for each analysis are  
71 shown in **Additional Supplementary File 5**.

72

73

74

75

76

77

78

79

80

81

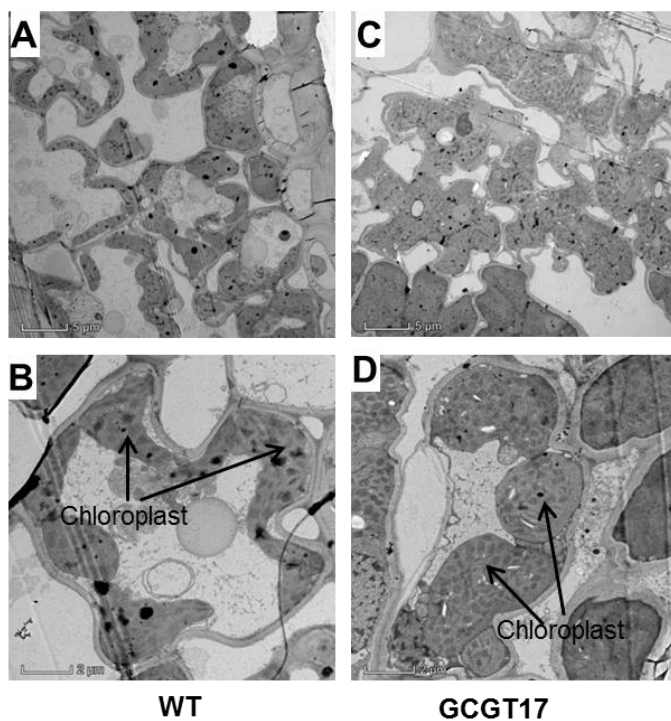
82

83

84

85 **Supplemental Figure 4**

86



87

88 **Supplemental Figure 4. Electron Micrographs of Leaf Sheaths of GCGT Transgenic Plants at**  
89 **the Filling Stage.**

90 (A, B) Transmission electron micrographs of leave sheaths in WT plants at the filling stage. (C, D)  
91 Transmission electron micrographs of leave sheaths in GCGT 17 at the filling stage. Each image is  
92 representative of four independent plants.

93

94

95

96

97

98

99

100

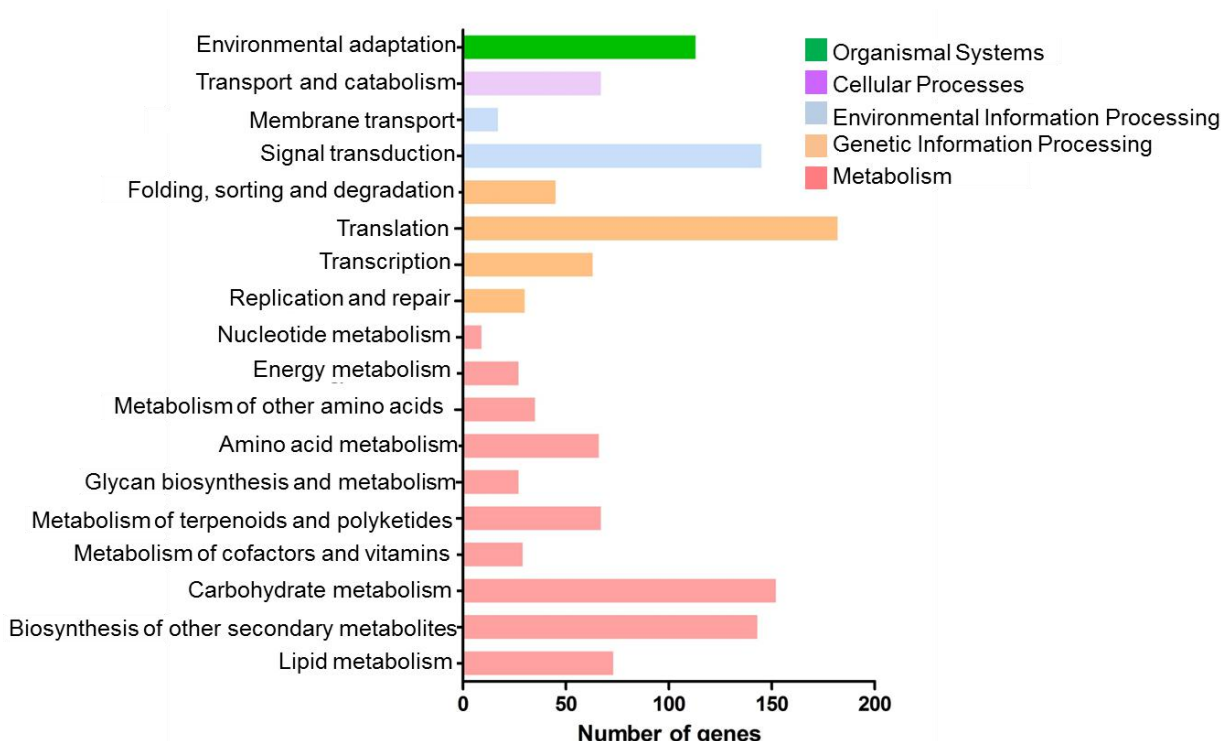
101

102

103

104 **Supplemental Figure 5**

105



106

107 **Supplemental Figure 5. KEGG Pathway Annotation Classification in the Stems of GCGT 12,**  
108 **17, and 20 versus WT Plants at the Filling Stage. (Fold change  $\geq 2.0$ , FDR  $< 0.05$ )**

109

110

111

112

113

114

115

116

117

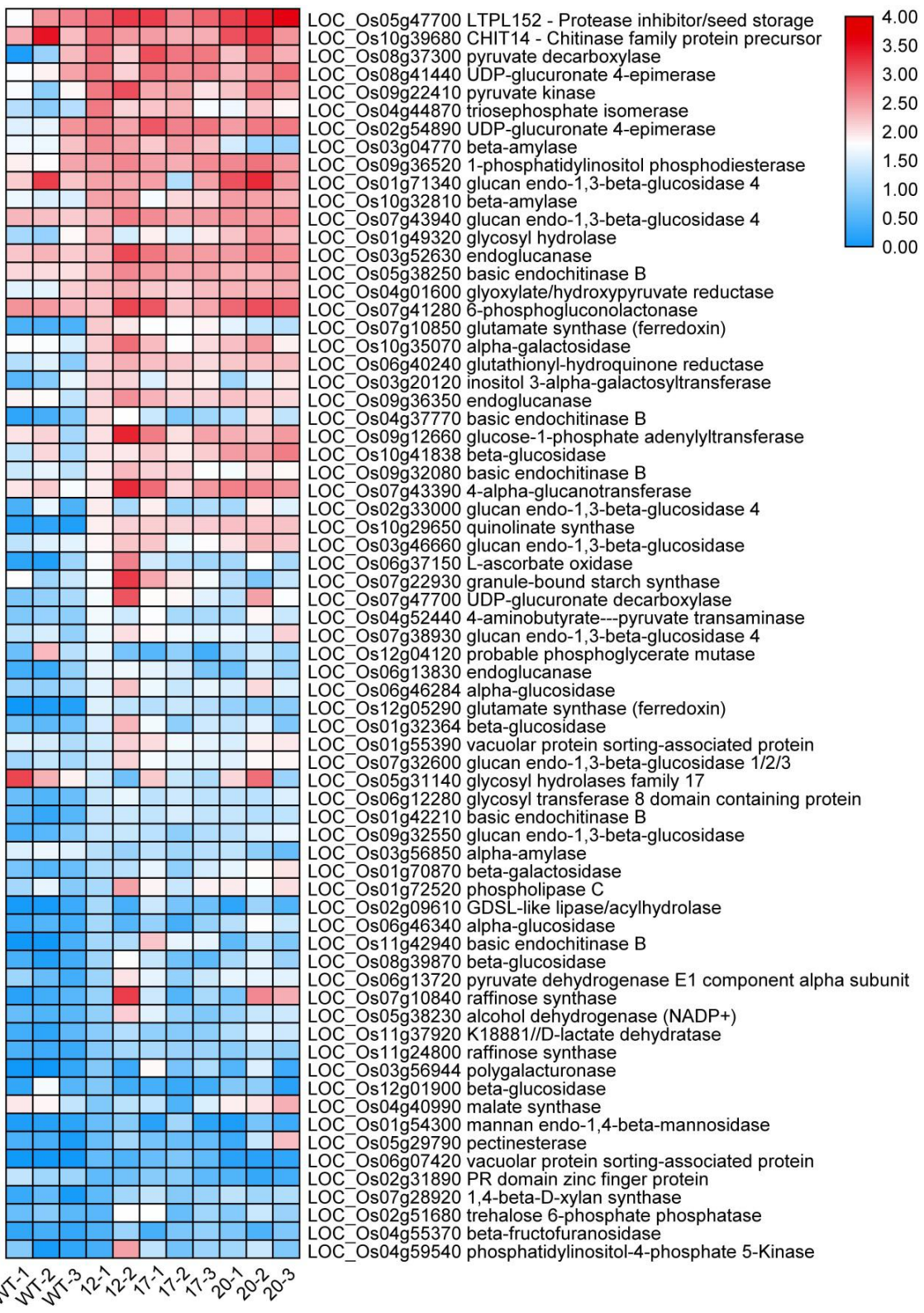
118

119

120

121

122 **Supplemental Figure 6**



Supplemental Table 1. Primers Used for RT-PCR

<i>Gene</i>	<i>Primer sequence</i>
<i>EcCAT</i>	5'- CGGCGAATTACGAACCGAAC-3' 5'- TTTGGCATGAACGCCTTG-3'
<i>OsGLO1</i>	5'- GAAGGCCTGGACCTCGCAGAG-3' 5'- CTAATGGTGATGGTGTGATGGCG-3'
<i>EcGCL</i>	5'- GTCGTCTGCCGTGTCGTA-3' 5'- CGGAATCGTCCAGCCTAA-3'
<i>EcTSR</i>	5'- TCATCATCATCATATCGAAGGTAGG-3' 5'- GCAGAACGGAATAGAGC-3'
<i>Actin</i>	5'- GACATTCAAGCGTTCCAGCCATGTAT-3' 5'- TGGAGCTTCCATGCCATGAGAGAA-3'

128

129

130   **Supplemental Table 2. Gas Exchange and Chlorophyll Fluorescence Parameters of GCGT and  
131   WT Plants**

132

	WT	GCGT 9	GCGT 12	GCGT 17	GCGT 20
<b>Light saturation point (LSP, <math>\mu\text{mol m}^{-2}\text{s}^{-1}</math>)</b>	1782 $\pm$ 35	2039 $\pm$ 58**	1985 $\pm$ 88**	1992 $\pm$ 115**	2121 $\pm$ 154**
<b>Dark respiration rate (Rd, <math>\mu\text{mol CO}_2</math> <math>\text{m}^{-2}\text{s}^{-1}</math>)</b>	0.88 $\pm$ 0.1	1.78 $\pm$ 0.09**	1.57 $\pm$ 0.1**	1.3 $\pm$ 0.17**	1.68 $\pm$ 0.08**
<b>Apparent quantum yield (AQE)</b>	0.068 $\pm$ 0.002	0.067 $\pm$ 0.007	0.064 $\pm$ 0.003	0.067 $\pm$ 0.006	0.063 $\pm$ 0.007
<b>Light-saturated photosynthetic rate (<math>A_{\max}</math>, <math>\mu\text{mol CO}_2 \text{m}^{-2}\text{s}^{-1}</math>)</b>	32.6 $\pm$ 0.4	37 $\pm$ 0.5**	36.4 $\pm$ 1.3**	37.7 $\pm$ 0.4**	35.7 $\pm$ 0.6**
<b>Carboxylation efficiency(CE)</b>	0.138 $\pm$ 0.009	0.167 $\pm$ 0.004*	0.166 $\pm$ 0.003*	0.159 $\pm$ 0.007*	0.156 $\pm$ 0.012*
<b>Apparent CO<sub>2</sub> compensation point(<math>\mu\text{mol}</math>)</b>	67.4 $\pm$ 1.1	62.2 $\pm$ 0.94*	60.9 $\pm$ 1.9*	62.8 $\pm$ 1.0*	65.7 $\pm$ 1.7
<b>Maximal photochemical efficiency of PSII (Fv/Fm)</b>	0.841 $\pm$ 0.01	0.839 $\pm$ 0.005	0.84 $\pm$ 0.009	0.842 $\pm$ 0.005	0.841 $\pm$ 0.007

133   The light-response curves and CO<sub>2</sub>-response curves were fit for calculating LSP, AQE, A<sub>max</sub>, CE, Rd, and Apparent  
134   CO<sub>2</sub> compensation point ( $n=4$ ). Leaves were dark adapted for at least 20 min prior to the measurement of Fv/Fm,  
135   ( $n=30$ ). Data are presented as the mean  $\pm$  SD; \*,  $P < 0.05$ ; \*\*,  $P < 0.01$ , according to one-way ANOVA, followed  
136   with a Tukey's posthoc test for means comparison. ANOVA tables for each analysis are shown in **Additional**  
137   **Supplementary File 5.**138   **Supplemental Table 3. Sizes and Numbers of Mesophyll Cells and Chloroplasts of GCGT and**

**WT Plants at the Filling Stage**

	<b>WT</b>	<b>GCGT17</b>
<b>Size of mesophyll cells (<math>\mu\text{m}^2</math>)</b>	$91.47 \pm 16.16$	$110.83 \pm 24.44^{**}$
<b>Size of chloroplasts (<math>\mu\text{m}^2</math>)</b>	$4.47 \pm 0.76$	$9.43 \pm 0.74^{**}$
<b>Number of mesophyll cells (per 1000 <math>\mu\text{m}^2</math>)</b>	$7.5 \pm 1.8$	$6.6 \pm 1.33$
<b>Number of chloroplasts (per 1000 <math>\mu\text{m}^2</math>)</b>	$42.29 \pm 3.9$	$41.46 \pm 4.88$
<b>Number of mitochondria (per 1000 <math>\mu\text{m}^2</math>)</b>	$30.09 \pm 6.1$	$30.7 \pm 5.1$

140 Sizes of mesophyll cells and chloroplasts ( $\mu\text{m}^2$ ),  $n=300$ ; numbers of mesophyll cells, chloroplasts, and  
 141 mitochondria (per 1000  $\mu\text{m}^2$ ),  $n=15$ . Data are presented as the mean  $\pm$  SD; \*\*,  $P < 0.01$ , according to one-way  
 142 ANOVA, followed with a Tukey's posthoc test for means comparison. ANOVA tables for each analysis are shown  
 143 in **Additional Supplementary File 5**.

144

145

146